

# *The role of the cloud radiative effect in the sensitivity of the Intertropical Convergence Zone to convective mixing*

Article

Accepted Version

Talib, J., Woolnough, S. J. ORCID: <https://orcid.org/0000-0003-0500-8514>, Klingaman, N. P. ORCID: <https://orcid.org/0000-0002-2927-9303> and Holloway, C. E. ORCID: <https://orcid.org/0000-0001-9903-8989> (2018) The role of the cloud radiative effect in the sensitivity of the Intertropical Convergence Zone to convective mixing. *Journal of Climate*, 31 (17). pp. 6821-6838. ISSN 1520-0442 doi: 10.1175/JCLI-D-17-0794.1 Available at <https://centaur.reading.ac.uk/77363/>

It is advisable to refer to the publisher's version if you intend to cite from the work. See [Guidance on citing](#).

To link to this article DOI: <http://dx.doi.org/10.1175/JCLI-D-17-0794.1>

Publisher: American Meteorological Society

All outputs in CentAUR are protected by Intellectual Property Rights law, including copyright law. Copyright and IPR is retained by the creators or other copyright holders. Terms and conditions for use of this material are defined in the [End User Agreement](#).

[www.reading.ac.uk/centaur](http://www.reading.ac.uk/centaur)

**CentAUR**

Central Archive at the University of Reading

Reading's research outputs online

1 **The role of the cloud radiative effect in the sensitivity of the Intertropical**  
2 **Convergence Zone to convective mixing.**

3 Joshua Talib \*

4 *Department of Meteorology, University of Reading, UK*

5 Steven J. Woolnough and Nicholas P. Klingaman

6 *National Centre for Atmospheric Science-Climate and Department of Meteorology, University of*  
7 *Reading, Reading, UK*

8 Christopher E. Holloway

9 *Department of Meteorology, University of Reading, UK*

10 \*Corresponding author address: Department of Meteorology, University of Reading, UK

11 E-mail: j.f.talib@pgr.reading.ac.uk

## ABSTRACT

12 Studies have shown that the location and structure of the simulated Intertrop-  
13 ical Convergence Zone (ITCZ) is sensitive to the treatment of sub-gridscale  
14 convection and cloud-radiation interactions. This sensitivity remains in ide-  
15 alised aquaplanet experiments with fixed surface temperatures. However,  
16 studies have not considered the role of cloud-radiative effects (CRE, atmo-  
17 spheric heating due to cloud-radiation interactions) in the sensitivity of the  
18 ITCZ to the treatment of convection. We use an atmospheric energy input  
19 (AEI) framework to explore how the CRE modulates the sensitivity of the  
20 ITCZ to convective mixing in aquaplanet simulations. Simulations show a  
21 sensitivity of the ITCZ to convective mixing, with stronger convective mixing  
22 favoring a single ITCZ. For simulations with a single ITCZ, the CRE main-  
23 tains the positive, equatorial AEI. To explore the role of the CRE further, we  
24 prescribe the CRE as either zero or a meridionally and diurnally varying cli-  
25 matology. Removing the CRE is associated with a reduced equatorial AEI  
26 and an increase in the range of convective mixing rates that produce a double  
27 ITCZ. Prescribing the CRE reduces the sensitivity of the ITCZ to convective  
28 mixing by 50%. In prescribed-CRE simulations, other AEI components, in  
29 particular the surface latent heat flux, modulate the sensitivity of the AEI to  
30 convective mixing. Analysis of the meridional moist static energy transport  
31 shows that a shallower Hadley circulation can produce an equatorward energy  
32 transport at low latitudes even with equatorial ascent.

## 33 **1. Introduction**

34 Tropical rainfall is often associated with a discontinuous zonal precipitation band commonly  
35 known as the Intertropical Convergence Zone (ITCZ). The ITCZ migrates between the Northern  
36 and Southern Hemispheres with the seasonal cycle, with a zonal-, time-mean position of approx-  
37 imately 6°N (Schneider et al. 2014). The ITCZ is co-located with the ascending branch of the  
38 Hadley circulation, where strong moist convection leads to high rainfall. The upper branches of  
39 the Hadley circulation typically transport energy poleward, away from the ITCZ. Recent studies  
40 have associated characteristics of the ITCZ with the energy transport by the Hadley circulation  
41 (Frierson and Hwang 2012; Donohoe et al. 2013; Adam et al. 2016; Bischoff and Schneider  
42 2016).

43 A double ITCZ bias is prominent in current and previous generations of coupled general  
44 circulation models (GCMs; Li and Xie 2014; Oueslati and Bellon 2015). The ITCZ is too  
45 intense in the Southern Hemisphere (Lin 2007), resulting in two annual-, zonal-mean tropical  
46 precipitation maxima, one in each hemisphere. A bias remains in atmosphere-only simulations  
47 with prescribed sea surface temperatures (SSTs) (Li and Xie 2014). Aquaplanet simulations  
48 provide an idealised modelling environment in which some complex boundary conditions in  
49 tropical circulation such as land/sea contrasts and orography are removed. However aquaplanet  
50 configurations of GCMs coupled to a slab ocean produce a broad range of tropical precipitation  
51 mean states (Voigt et al. 2016); even prescribing zonally uniform SSTs does not resolve the  
52 inter-model variability (Blackburn et al. 2013).

53

54 *a. Modelling studies*

55 Characteristics of the simulated ITCZ are sensitive to the representation of cloud-radiation inter-  
56 actions (Fermepin and Bony 2014; Li et al. 2015; Harrop and Hartmann 2016). In the deep tropics  
57 the cloud radiative effect (CRE) warms the atmosphere (Allan 2011), with important effects on  
58 tropical circulation (Slingo and Slingo 1988; Crueger and Stevens 2015). The CRE is associated  
59 with a more prominent single ITCZ (Crueger and Stevens 2015; Harrop and Hartmann 2016; Popp  
60 and Silvers 2017). Both Harrop and Hartmann (2016) and Popp and Silvers (2017) investigated  
61 the association between the Hadley circulation and CRE in a range of aquaplanet simulations with  
62 and without the CRE. In all GCMs used, the CRE is associated with increased equatorial rainfall,  
63 an equatorward contraction of the ITCZ, and a strengthening of the mean meridional circulation.  
64 The authors emphasise different mechanisms by which the CRE promotes a single ITCZ. Harrop  
65 and Hartmann (2016) propose that the CRE warms the upper tropical troposphere, which reduces  
66 the convective available potential energy and restricts deep convection to the region of warmest  
67 SSTs, whilst Popp and Silvers (2017) argue that the CRE strengthens the Hadley circulation and  
68 moves the ITCZ equatorward, associated with increased moist static energy (MSE) advection by  
69 the lower branches of the Hadley circulation. The strengthening of the mean circulation is asso-  
70 ciated with the CRE meridional gradient, as the CRE is positive in the tropics and negative in the  
71 extra-tropics ( $\geq \pm 45^\circ$  latitude; Allan 2011). However, it should be noted that the CRE reduces  
72 total tropical-mean ( $\leq \pm 30^\circ$  latitude) precipitation due to reduced radiative cooling (Harrop and  
73 Hartmann 2016).

74 Across a hierarchy of models it has been shown that the simulation of tropical precipitation  
75 is sensitive to the representation of convection (Terray 1998; Frierson 2007; Wang et al. 2007;  
76 Chikira 2010; Mobis and Stevens 2012; Oueslati and Bellon 2013; Bush et al. 2015; Nolan et al.

77 2016). For example, variations in lateral entrainment and detrainment rates, which alter the repre-  
78 sentation of deep convection, affect the diurnal cycle of precipitation over the Maritime Continent  
79 (Wang et al. 2007) and South Asian monsoon precipitation rates (Bush et al. 2015). Increasing  
80 convective mixing strengthens deep convection in convergence zones, associated with an increased  
81 moisture flux from subsidence regions (Terray 1998; Oueslati and Bellon 2013).

82 In full GCMs, complex surface characteristics and boundary conditions including land-sea con-  
83 trasts, orography and SST gradients, make it challenging to understand the sensitivity of tropical  
84 precipitation to the representation of convection (Oueslati and Bellon 2013; Bush et al. 2015).  
85 Even in the absence of complex surface topography, aquaplanet studies have also shown that  
86 characteristics of tropical precipitation, in particular the location and intensity of the ITCZ, are  
87 sensitive to the sub-gridscale treatment of convection (Hess et al. 1993; Numaguti 1995; Chao  
88 and Chen 2004; Liu et al. 2010; Mobis and Stevens 2012). Mobis and Stevens (2012) studied the  
89 sensitivity of the ITCZ location to the choice of convective parameterisation scheme in an aqua-  
90 planet configuration of the ECHAM GCM by comparing the Nordeng (1994) and Tiedtke (1989)  
91 schemes, which vary in their formulations of entrainment, detrainment and cloud base mass flux  
92 for deep convection. The Nordeng scheme, with a higher lateral entrainment rate, produced a  
93 single ITCZ, whilst the Tiedtke scheme produced a double ITCZ. The authors associate the loca-  
94 tion of maximum boundary layer MSE with the ITCZ location; they argue that mechanisms that  
95 control the boundary layer MSE are important to the sensitivity of the ITCZ to the representation  
96 of convection. The boundary layer MSE distribution is predominantly controlled by the surface  
97 winds, which are influenced by convective heating, allowing variations in convective heating to  
98 influence the ITCZ structure. The importance of the surface winds is further emphasised by simu-  
99 lations with prescribed surface winds in the computation of the surface fluxes (Mobis and Stevens  
100 2012). These simulations lead to the conclusion that there is a strong association between surface

101 turbulent fluxes and the ITCZ.

102 While the ITCZ has been shown to be sensitive to the CRE and the convective parameterisation  
103 scheme, no study has separated these effects. This paper will analyse the sensitivity of the ITCZ to  
104 convective mixing in aquaplanet simulations using the Met Office Unified Model (MetUM), and  
105 the role of the CRE in this sensitivity.

### 106 *b. Atmospheric Energy framework*

107 Literature based on a hierarchy of models, as well as reanalysis data and observations, concludes  
108 that the northward displacement of the ITCZ from the equator is anti-correlated with the north-  
109 ward cross-equatorial atmospheric energy transport (Kang et al. 2008; Frierson and Hwang 2012;  
110 Donohoe et al. 2013). Bischoff and Schneider (2014) developed a diagnostic framework to relate  
111 the location of the ITCZ to this energy transport.

112 The zonal-mean atmospheric MSE budget is (Neelin and Held 1987):

$$[AEI] = \partial_t[\hat{h}_e] + \partial_y[\hat{v}h] \quad (1)$$

113 where  $AEI$  is the atmospheric energy input (AEI);  $vh$  is the meridional MSE flux, ( $v$  is meridional  
114 wind;  $h$  is MSE);  $h_e$  is the moist enthalpy;  $[\ ]$  denotes a zonal- and time-mean;  $\hat{\ }^$  represents a mass  
115 weighted vertical integral;  $\partial_y$  is the meridional derivative; and  $\partial_t$  is the time derivative. Local  
116 Cartesian coordinates are printed with  $y = a\phi$ , (where  $a$  is Earth's radius and  $\phi$  is latitude,) but  
117 all calculations are performed in spherical coordinates. Bischoff and Schneider (2014) assume  
118 a statistically steady state ( $\partial_t[\hat{h}_e]=0$ ) and that  $[\hat{v}h]$  in the tropics is dominated by the zonal-mean  
119 circulation and therefore  $[\hat{v}h]$  equals zero at the ITCZ. Through performing a first-order Taylor  
120 expansion of the equatorial  $[\hat{v}h]$ , Bischoff and Schneider (2014) derive the dependence of the  
121 ITCZ location on the equatorial MSE flux and equatorial AEI:

$$\delta \approx -\frac{1}{a} \frac{[\widehat{vh}]_0}{[AEI]_0} \quad (2)$$

122 with the AEI defined as:

$$[AEI] = [S] - [L] - [O] \quad (3)$$

123 where subscript 0 denotes the equatorial value,  $S$  is the net incoming shortwave radiation at the  
 124 top of the atmosphere (TOA),  $L$  is the outgoing longwave radiation at the TOA, and  $O$  is the net  
 125 downward flux at the surface. Bischoff and Schneider (2016) retain higher order terms in the  
 126 Taylor expansion to derive a framework for negative  $[AEI]_0$ . A negative  $[AEI]_0$  is associated with  
 127 a double ITCZ as  $[\widehat{vh}]$  no longer increases with latitude; energy is transported equatorward at low  
 128 latitudes to achieve equilibrium. A double ITCZ is associated with two off-equatorial energy flux  
 129 equators, where the total meridional energy flux equals zero. Bischoff and Schneider (2016) derive  
 130 an expression for the locations of a double ITCZ:

$$\delta \approx \pm \frac{1}{a} \left\{ -\frac{6([AEI]_0)}{\partial_{yy}([AEI]_0)} \right\}^{\frac{1}{2}} + \frac{[\widehat{vh}]_0}{2a([AEI]_0)} \quad (4)$$

131 Note equation 4 is from a corrigendum for the original paper.

132 Bischoff and Schneider (2014) explore the relationship derived in (2) using an idealised slab-  
 133 ocean GCM with a prescribed oceanic heat transport. They investigate the effects of the  $[AEI]_0$  and  
 134 the  $[\widehat{vh}]_0$  through varying the imposed equatorial ocean heat flux and the atmospheric longwave  
 135 absorption. Changes in both  $[AEI]_0$  and  $[\widehat{vh}]_0$  affect the latitude of the ITCZ; this theoretical rela-  
 136 tionship is supported in observations and reanalyses (Adam et al. 2016). Bischoff and Schneider  
 137 (2016) examine the double ITCZ framework (4) using a slab-ocean GCM and varying the tropical  
 138 and extra-tropical components of the imposed ocean energy flux divergence. An increased tropical  
 139 ocean energy flux divergence decreases the  $[AEI]_0$ . For double ITCZ scenarios and when  $[\widehat{vh}]_0$  is  
 140 negligible, decreasing the  $[AEI]_0$  shifts the energy flux equator poleward. The diagnosed energy

141 flux equators from (2) and (4) are close to the simulated precipitation maxima, highlighting the  
142 association between the AEI and ITCZ.

143 However, Bischoff and Schneider (2014)’s definition of the  $[AEI]$  (3) is chosen as their simu-  
144 lations prescribe  $O$ , which allows only the TOA energy budget ( $S - L$ ) to vary. This constrains  
145 the AEI response to model perturbations, as surface radiation and turbulent fluxes are constrained  
146 at equilibrium, which could reduce the impact of surface-flux feedbacks on the ITCZ. We use  
147 atmosphere-only simulations with prescribed SSTs, allowing variations in the components of  $O$ .  
148 As our experiments do not have a closed surface energy balance and we are interested in cloudy-  
149 sky radiation AEI components, we choose to write the AEI as:

$$[AEI] = [SW] + [LW] + [H] \quad (5)$$

150 where  $SW$  and  $LW$  represent the net atmospheric heating from shortwave and longwave radiation,  
151 respectively, and  $H$  denotes the atmospheric heating from surface sensible and latent heat fluxes.  
152 Both fixed SST and prescribed  $O$  frameworks misrepresent the real climate system by restricting  
153 air-sea coupled feedbacks (discussed further in section 4). From an AEI perspective, Mobis and  
154 Stevens (2012) severely constrain  $H$  in a subset of experiments by prescribing the surface winds  
155 when computing the surface fluxes. This reduces the sensitivity of the ITCZ to the convective  
156 parameterisation scheme.

157 Previous research on the response of the simulated ITCZ to variations in the sub-gridscale rep-  
158 resentation of convection have not considered the role of the CRE or used an energy budget frame-  
159 work like that proposed by Bischoff and Schneider (2014). We hypothesise that the sensitivity of  
160 the ITCZ to these factors can be linked to variations in AEI and  $[\widehat{vh}]$ .

## 161 2. Methodology

162 We use variations of an N96 (1.25° latitude × 1.875° longitude) aquaplanet configuration of the  
163 Met Office Unified Model (MetUM) Global Atmosphere 6.0 (GA6.0) configuration (Walters et al.  
164 2017). The deep convective parameterisation scheme is an altered form of the mass flux scheme  
165 in Gregory and Rowntree (1990), including a convective available potential energy closure based  
166 on Fritsch and Chappell (1980) and a mixing detrainment rate dependent on the relative humidity  
167 (Derbyshire et al. 2004). Unless noted, all simulations are run for three years with a “Qobs” SST  
168 profile (Neale and Hoskins 2001), with the first sixty days discarded as spin-up.

### 169 *a. Simulations performed*

170 To explore the sensitivity of the simulated ITCZ to convective mixing, we perform five simu-  
171 lations varying the lateral entrainment ( $\varepsilon$ ) and detrainment ( $d_m$ ) rates for deep-level convection  
172 (Table 1). In GA6.0 these rates are:

$$\varepsilon = 4.5 f_{dp} \frac{p(z)\rho(z)g}{p_*^2} \quad (6)$$

$$d_m = 3.0(1 - RH)\varepsilon \quad (7)$$

174 Both  $\varepsilon$  and  $d_m$  are given as a fractional mixing rate per unit length ( $m^{-1}$ ). In (6) and (7),  $p$  and  
175  $p_*$  are pressure and surface pressure ( $Pa$ );  $\rho$  is density ( $kg\ m^{-3}$ );  $g$  is gravitational acceleration  
176 ( $m\ s^{-2}$ );  $f_{dp}$  is a constant with the default value of 1.13;  $RH$  is relative humidity. We control  $\varepsilon$   
177 and  $d_m$  by scaling  $f_{dp}$  to five values between 0.25 and  $1.5 \times$  the default value: 0.28 (F0.28), 0.57  
178 (F0.57), 0.85 (F0.85), 1.13 (F1.13) or 1.70 (F1.70).

179 To explore the influence of the CRE on the sensitivity of the ITCZ to convective mixing we  
180 perform a companion set of experiments with cloud-radiation interactions removed: F0.28NC,

181 F0.57NC, F0.85NC, F1.13NC and F1.70NC (Table 1). Cloud-radiation interactions are removed  
182 by setting the cloud liquid and cloud ice to zero in the radiation scheme.

183 Finally, a third set of simulations use a prescribed CRE (Table 2) to investigate the relative  
184 importance of  $f_{dp}$  and the CRE to characteristics of the ITCZ. The four simulations have a pre-  
185 scribed, diurnally varying CRE vertical profile computed from a single-year simulation with  $f_{dp}$   
186 equal to 0.57 or 1.13 (PC0.57 and PC1.13, respectively). The CRE is prescribed using cloudy-sky  
187 upward and downward fluxes at each model level at every model timestep. The diurnally varying  
188 CRE profile is computed as a hemispherically symmetric and zonally uniform composite of the  
189 climatological diurnal cycle at each grid point, referenced to local solar time. Two of the four  
190 simulations prescribe a CRE at a different  $f_{dp}$  constant from that in the simulation (F1.13PC0.57,  
191 F0.57PC1.13), whilst the other two simulations use a CRE from the same  $f_{dp}$  value to assess the  
192 sensitivity to prescribing cloud-radiation interactions (F1.13PC1.13, F0.57PC0.57).

### 193 3. Results

#### 194 a. Sensitivity of the ITCZ to the convective mixing.

195 Figure 1a shows the sensitivity of the ITCZ to  $f_{dp}$  with a single ITCZ at higher values (F1.13,  
196 F1.70). Reducing  $f_{dp}$  promotes a double ITCZ, with peak precipitation further away from the  
197 equator (F0.28, F0.57). F0.85 has a marginal double ITCZ with no substantial difference between  
198 equatorial and off-equatorial precipitation. Decreasing  $f_{dp}$  is associated with a weaker horizontal  
199 gradient of the mass meridional streamfunction (Figure 2). F0.28 is the only simulation to  
200 show a reversed Hadley circulation in the deep tropics (Figure 2e), associated with upper-level  
201 zonal-mean equatorial subsidence, typical of a double ITCZ. F0.57 meanwhile has a typical  
202 double ITCZ structure in precipitation but not in the mass meridional streamfunction (Figure 1a

203 and 2d), which we refer to as a “split ITCZ”: two off-equatorial precipitation maxima and two  
204 ascending branches of the Hadley circulation, without any substantial zonal-mean subsidence  
205 equatorward of the precipitation maxima.

206 Convective mixing reduces the difference in MSE between a convective plume, determined by  
207 the boundary layer MSE, and the free-troposphere (Mobis and Stevens 2012), which reduces the  
208 buoyancy of the convective plume. Assuming the sensitivity of the environmental saturated MSE  
209 to  $f_{dp}$  is small, the depth of convection will depend on the boundary layer MSE and  $f_{dp}$ . De-  
210 creasing  $f_{dp}$  will deepen convection for a constant boundary layer MSE, and reduce the minimum  
211 boundary layer MSE at which deep convection occurs. Following weak-temperature gradient  
212 arguments (e.g. Sobel et al. 2001) and assuming a small meridional gradient in free-tropospheric  
213 tropical temperature, and hence a small gradient in the saturated MSE across the deep tropics,  
214 the reduced minimum boundary layer MSE needed for deep convection strengthens convection  
215 in off-equatorial tropical latitudes over cooler SSTs. Stronger off-equatorial deep convection  
216 decreases equatorward low-level winds in the deep tropics, reducing equatorial boundary layer  
217 MSE. Hence, decreasing  $f_{dp}$  is associated with a poleward ITCZ shift and promotes a double  
218 ITCZ. Similar arguments can be made for higher  $f_{dp}$  promoting a single ITCZ.

219 The sensitivity of the ITCZ to  $f_{dp}$  is associated with AEI changes (Figure 1b), with a change  
220 from a single (F1.13) to a double/split ITCZ (F0.28/F0.57) associated with a decrease in the  $[AEI]_0$   
221 (Figure 3d and e). Simulations with a single/double ITCZ in precipitation have a positive/negative  
222  $[AEI]_0$  (Figure 1b), in agreement with Bischoff and Schneider (2014). Changes in cloudy-sky  
223 radiation and latent heat flux are the dominant components of AEI changes (blue and orange  
224 lines, respectively, in Figure 3). In F1.13 the total CRE peaks at approximately  $60 \text{ Wm}^{-2}$  at the  
225 equator and reduces to zero around  $15^\circ$  latitude (blue line in Figure 3b). This equatorial warming  
226 comes almost entirely from the longwave CRE, which dominates the total CRE equatorward

227 of  $10^\circ$  latitude (not shown). In the subtropics,  $20^\circ$  to  $30^\circ$  latitude, low clouds contribute to a  
 228 negative CRE of  $\approx 2 \text{ Wm}^{-2}$ , as longwave cooling from boundary layer clouds is greater than  
 229 the shortwave heating. Without the CRE contribution to the  $[AEI]_0$  in F1.13,  $[AEI]_0$  would be  
 230 negative, suggesting that the CRE maintains the single ITCZ. Removing the CRE from the AEI  
 231 in F1.13 would give an  $[AEI]_0$  of  $-25.7 \text{ Wm}^{-2}$ , assuming that no other AEI components change.  
 232 Using Bischoff and Schneider (2016)'s framework, (4), with values for AEI once removing  
 233 the CRE and assuming that  $[\widehat{v\bar{h}}]_0 \simeq 0 \text{ Wm}^{-1}$ , (associated with an hemispherically symmetric  
 234 atmospheric circulation), predicts a double ITCZ at  $\pm 5.6^\circ$  latitude.

235 The split ITCZ in F0.57 is associated with a substantially reduced equatorial CRE and an  
 236 increased off-equatorial CRE (Figure 3d). We chose CRE profiles from one year of F0.57 and  
 237 F1.13 for our prescribed CRE simulations (Table 2), as these two simulations show CRE profiles  
 238 typical of a double and single ITCZ, respectively; these simulations are analysed in section 3d.  
 239 As the Hadley circulation and ITCZ are associated with the AEI, and the CRE plays a substantial  
 240 role in AEI changes when varying  $f_{dp}$ , we hypothesize that prescribing the CRE will reduce or  
 241 remove the sensitivity of the AEI and ITCZ to  $f_{dp}$ .

242

### 243 *b. Sensitivity of the ITCZ to convective mixing with no cloud radiative effect*

244 To test our hypothesis above, we first analyse simulations with the CRE removed (Table  
 245 1), similar to Harrop and Hartmann (2016). Figure 4a and Figure 5 show the zonal-mean  
 246 precipitation and mass meridional streamfunction respectively in simulations with no CRE (Table  
 247 1). Removing the CRE at  $f_{dp} = 1.13$  (F1.13NC) leads to a switch from a single to a split ITCZ,  
 248 and a  $\approx 20\%$  weakening of the Hadley circulation (Figure 4a and 5b).

249 Similar to Harrop and Hartmann (2016), removing the CRE cools the tropical ( $\leq 30^\circ$  latitude)

250 upper-troposphere, destabilizing the atmosphere and reducing the environmental saturated  
251 MSE. For a fixed boundary layer MSE and convective mixing rate, removing the CRE deepens  
252 convection as the buoyancy of a convective plume increases relative to the saturated MSE of the  
253 environment. Hence, removing the CRE reduces the minimum boundary layer MSE for deep  
254 convection, strengthening off-equatorial convection over cooler SSTs. Stronger off-equatorial  
255 convection decreases equatorward low-level winds in the deep tropics, reducing equatorial  
256 boundary layer MSE and promoting a double ITCZ. This mechanism is similar to that proposed  
257 for the sensitivity of the ITCZ to  $f_{dp}$  (section 3a). However, when removing the CRE changes in  
258 the environmental saturated MSE play the dominant role, whilst for the sensitivity of the ITCZ to  
259  $f_{dp}$ , changes in the convective parcel MSE dominate.

260 The weaker Hadley circulation and double ITCZ in precipitation in F1.13NC is consistent  
261 with AEI changes. In F1.13NC removing CRE reduces the  $[AEI]_0$  by  $\approx 45 \text{ Wm}^{-2}$ , leading to a  
262 negative  $[AEI]_0$ , and increases the subtropical AEI by up to  $15 \text{ Wm}^{-2}$  (20 to  $45^\circ$  latitude) (Figure  
263 6f). Across the deep tropics the AEI change is not equal to the CRE diagnosed from F1.13, due to  
264 increased turbulent and clear-sky fluxes. These increased fluxes, associated with an equatorward  
265 shift of the ITCZ, partially offset the reduction in  $[AEI]_0$ . Hence, the predicted location of the  
266 double ITCZ in section 3a when removing the CRE overestimated the poleward shift of the  
267 ITCZ. Removing the CRE reduces tropical-domain ( $\leq 30^\circ$  latitude) AEI, which is associated  
268 with increased AEI at higher latitudes to maintain equilibrium. Our simulations are consistent  
269 with the suggested mechanisms proposed by Popp and Silvers (2017): the ITCZ is located at the  
270 maximum boundary layer MSE, and a weaker meridional circulation is associated with a reduced  
271 AEI gradient.

272 At all  $f_{dp}$  removing the CRE reduces the maximum precipitation rate, weakens the Hadley  
273 circulation (comparing Figure 1a and 4a), and moves the latitude of peak precipitation poleward

274 (Figure 7a). The sensitivity of the ITCZ structure to removing the CRE depends on the convective  
275 mixing rate: either a broader single ITCZ (F1.70NC), a poleward shift of a double/split ITCZ  
276 (F0.28NC and F0.57NC), or a switch from a single to a split/double ITCZ (F0.85NC and  
277 F1.13NC). Removing the CRE cools the upper troposphere and reduces the boundary layer MSE  
278 required for deep convection. This increases the  $f_{dp}$  value at which the ITCZ transitions from  
279 single to split/double.

280 Removing the CRE changes, but does not remove, the sensitivity of the ITCZ to  $f_{dp}$ . Quan-  
281 tifying the apparent effect of the CRE on the sensitivity of the ITCZ to  $f_{dp}$  is difficult, as the  
282 effect depends on both the range of  $f_{dp}$  considered and the metric used (Figure 7). When an  
283 off-equatorial ITCZ is simulated in CRE-off simulations ( $0.28 \leq f_{dp} \leq 1.13$ ), including the CRE  
284 increases the sensitivity of the ITCZ location to  $f_{dp}$  by  $\approx 30\%$  (comparing the slopes of the solid  
285 regression lines in Figure 7a). However, because F1.70NC has a single ITCZ, including the CRE  
286 cannot shift the ITCZ equatorward. Hence, when  $0.28 \leq f_{dp} \leq 1.70$  the change in sensitivity  
287 reduces to nearly zero (comparing the slopes of the dashed lines). The reduction in sensitivity  
288 also depends on the chosen metric; for instance, the maximum precipitation rate has a negligible  
289 sensitivity to  $f_{dp}$  in CRE-off simulations but a substantial sensitivity in CRE-on simulations  
290 (Figure 7b), highlighting that the CRE has a positive feedback on convection as increasing  $f_{dp}$  is  
291 associated with an increased CRE (Figure 8).

292 Increasing  $f_{dp}$  is associated with an increased tropical-domain CRE (Figure 8), which is  
293 counter-intuitive as one might expect that increasing  $f_{dp}$  will lead to lower cloud tops and  
294 hence a reduced CRE. However, the maximum cloud top height at the ITCZ is insensitive to  
295  $f_{dp}$  (not shown), but the minimum temperature where the cloud fraction goes to zero (cloud top  
296 temperature) is sensitive to  $f_{dp}$  in both CRE-on and CRE-off simulations (Figure 8). The cloud  
297 top temperature decreases as  $f_{dp}$  increases (Figure 8), associated with a cooler upper-troposphere.

298 Furthermore, the increase in SST at the ITCZ location, associated with equatorward contraction  
299 of the ITCZ, also contributes to an increased CRE at higher  $f_{dp}$ .

300 Removing the CRE decreases the sensitivity of the AEI to  $f_{dp}$  (comparing Figure 1b and  
301 Figure 4b). The reduced sensitivity of the AEI is associated with a reduced sensitivity of the  
302 ITCZ. Latent heat flux variations account for most of the remaining AEI sensitivity to  $f_{dp}$   
303 (Figure 6). In simulations with a double ITCZ (F0.28NC, F0.57NC and F0.85NC), changes in  
304 the latent heat flux and AEI have a bi-modal structure, indicating reduced latent heat flux at the  
305 location of maximum precipitation in F1.13NC (Figure 6c-e). Changes in the latent heat flux  
306 are predominantly controlled by alterations in near-surface wind speed rather than changes in  
307 near-surface specific humidity (not shown).

308 Simulations so far agree with the association in Bischoff and Schneider (2016) between a neg-  
309 ative  $[AEI]_0$  and a double ITCZ. However, the negative  $[AEI]_0$  in F0.57, F0.85NC and F1.13NC  
310 requires an equatorward transport of energy at low latitudes, but the mean mass meridional  
311 streamfunction suggests a poleward transport of energy (Figure 2b, 5c, 5d). In the following  
312 subsection we discuss mechanisms for an equatorward energy transport.

313

### 314 *c. Mechanisms responsible for an equatorward energy transport*

315 To better understand the response of the mean circulation, associated with ITCZ changes, to  
316 varying  $f_{dp}$  and removing the CRE, we partition the divergence of the MSE flux ( $\partial_y[\widehat{v\hat{h}}]$ ) into  
317 two components: the mean circulation ( $\partial_y([\widehat{v}][\widehat{h}])$ ) and the eddy contribution ( $\partial_y[\widehat{v\hat{h}}] - \partial_y([\widehat{v}][\widehat{h}])$ ).  
318 In these simulations it has not been possible to close the atmospheric energy budget (1) due to  
319 local energy conservation issues (discussed further in section 4), however the sign of the  $[AEI]_0$   
320 is consistent with the sign of the  $\partial_y[\widehat{v\hat{h}}]$  in simulations so far. In all simulations the eddy con-

321 tribution to the meridional MSE flux is substantial across the tropics highlighting that the mean  
 322 atmospheric circulation is not solely responsible for transporting energy. Furthermore, one should  
 323 not necessarily assume a correspondence between the required MSE transport and the transport  
 324 by the mean meridional circulation. In simulations with a single/double ITCZ, both the mean cir-  
 325 culation and eddies transport energy poleward/equatorward at low latitudes. In F0.57, which has  
 326 a negative  $[AET]_0$  and a split ITCZ, equatorward transport of energy at low latitudes is achieved  
 327 solely by eddies. When  $f_{dp}$  equals 0.85 and 1.13, a change in the sign of the energy transport by  
 328 the mean circulation ( $\partial_y([\hat{v}][\hat{h}])$ ) occurs at low latitudes when removing the CRE, however there is  
 329 still equatorial ascent across most of the troposphere (Figure 5b, c). To understand the sensitivity  
 330 of the mean circulation to removing the CRE at these convective mixing rates, we partition the  
 331 change in the MSE flux ( $[\hat{v}][\hat{h}]$ ) into mean circulation changes and MSE variations.

332 First, the meridional mass flux, denoted by  $V$ , in F1.13NC ( $V_e$ ) is partitioned into two compo-  
 333 nents:

$$\begin{aligned}
 V_e &= V_c(1 + \alpha) + V_r \\
 \text{where } \alpha &= \frac{V_e \cdot V_c}{V_c \cdot V_c} - 1
 \end{aligned}
 \tag{8}$$

334 Subscripts  $c$  and  $e$  represent the zonal-, time-mean value of the control and experiment simulation  
 335 (in this case F1.13 and F1.13NC respectively).  $\alpha$  is a globally uniform scaling term calculated  
 336 using the dot product of the meridional mass fluxes in the tropics (30°N to 30°S). We account for  
 337 variations in density in  $V$ .  $V_c(1 + \alpha)$  represents a change in strength of the control circulation;  $V_r$   
 338 represents a change in circulation structure. Next, the MSE,  $(c_p T + gz + Lq)$ , in the experiment  
 339 simulation ( $h_e$ ) is written as:

$$h_e = h_c + h_p
 \tag{9}$$

340 where subscript  $p$  represents the zonal-, time-mean difference between the two simulations. The  
 341 change in the MSE flux between the experiment and control simulation can therefore be written  
 342 as:

$$V_e h_e - V_c h_c = \alpha V_c h_c + V_r h_c + V_c h_p + (\alpha V_c + V_r) h_p \quad (10)$$

343 Each term in (10) represents a mechanism by which  $vh$  can vary:  $\alpha V_c h_c$  represents circulation  
 344 intensity changes;  $V_r h_c$  represents changes in circulation structure;  $V_c h_p$  represents MSE profile  
 345 changes; and  $(\alpha V_c + V_r) h_p$ , represents MSE profile changes correlated with changes in circulation  
 346 structure and strength.

347 Three out of the four mechanisms are important in reducing the poleward MSE transport by  
 348 the Hadley circulation in F0.85NC and F1.13NC (Figure 9): a reduction in Hadley circulation  
 349 strength (Figure 9e); a shallower mean circulation (Figure 9f); and a reduced MSE export at  
 350 the top of the Hadley circulation due to lower MSE associated with upper-tropospheric cooling  
 351 (Figure 9g). MSE profile changes correlated with changes in circulation strength and intensity  
 352  $[(\alpha V_c + V_r) h_p]$  are small compared to the other three mechanisms (Figure 9h). As changes  
 353 in circulation strength ( $\alpha V_c h_c$ ) cannot change the direction of energy transport, the reduced  
 354 upper-tropospheric MSE ( $V_c h_p$ ) and shallower Hadley circulation ( $V_r h_c$ ) must be responsible  
 355 for the change in energy transport direction by the mean circulation. At the equator, circulation  
 356 strength changes ( $\alpha V_c h_c$ ) contribute  $\approx 16\%$  of the reduced  $\partial_y([\hat{v}][\hat{h}])$ ; reduced MSE export by the  
 357 upper branch of the mean circulation ( $V_c h_p$ ) and a shallower Hadley circulation ( $V_r h_c$ ) contribute  
 358  $\approx 34\%$  and  $50\%$  respectively (not shown). Therefore, at certain convective mixing rates, in our  
 359 case when  $f_{dp} = 0.85$  and  $1.13$ , removing the CRE is not associated with a substantial double  
 360 ITCZ in the mass meridional streamfunction, even though MSE is transported equatorward at

low latitudes and the  $[AEI]_0$  is negative. Similar behaviour has also been concluded by Popp and Silvers (2017) who found that in certain simulations the zero mass meridional streamfunction remained at the equator even when the  $[AEI]_0$  was negative.

Removing the CRE and varying  $f_{dp}$  are associated with substantial AEI changes which require MSE transport variations. In the two sets of simulations discussed so far, we identified three mechanisms to transport MSE equatorward at low latitudes; which mechanisms dominates depends on the CRE and  $f_{dp}$ . First, in F0.28, F0.28NC and F0.57NC, subsidence across the equatorial region is associated with an equatorward MSE flux at low latitudes (Figure 2e and Figure 5d, e). Secondly, eddy energy transport plays a role in the equatorward MSE flux in F0.28, F0.57, F0.28NC, F0.57NC, F0.85NC. Thirdly, in F0.85NC and F1.13NC a shallower Hadley circulation and reduced upper-tropospheric MSE reduces the MSE exported in the upper branches of the mean circulation, resulting in a net equatorward MSE transport. All other simulations (F0.85, F1.13, F1.70 and F1.70NC) have a single ITCZ associated with a positive  $[AEI]_0$  and poleward MSE transport at low latitudes.

#### *d. Sensitivity of the ITCZ to convective mixing with a prescribed cloud radiative effect.*

To further understand the role of the CRE on the sensitivity of the ITCZ to convective mixing, we perform prescribed-CRE simulations and vary  $f_{dp}$  (Table 2). The prescribed CRE is diagnosed from single-year simulations with  $f_{dp}$  equal to 1.13 or 0.57 (section 2). The effect of prescribing the diurnal cycle of the CRE in a simulation with the same  $f_{dp}$  is minimal; for example, the ITCZ is similar in F1.13PC1.13 and F1.13 (Figure 1 and 10). Hence, we only discuss the mean circulation in F1.13PC0.57 and F0.57PC1.13 (Figure 11a and c).

Similar to CRE-off simulations, the sensitivity of the ITCZ to  $f_{dp}$  reduces in prescribed CRE

384 simulations (Figure 10a) compared to CRE-off simulations (Figure 1a), associated with a reduced  
385 sensitivity of the AEI to  $f_{dp}$  (Figure 10b, 12a and c). The prescribed CRE heating acts as a fixed  
386 MSE source, which requires an increase in MSE export and hence increased convective activity.  
387 In PC1.13 simulations the CRE maximises at the equator, which is associated with increased  
388 equatorial convective activity and a single ITCZ. In PC0.57 simulations on the other hand, the  
389 CRE peaks off the equator and promotes a double ITCZ. The root mean squared difference of  
390 tropical precipitation and the mass meridional streamfunction illustrates that prescribing the  
391 CRE reduces the sensitivity of the ITCZ and Hadley circulation to  $f_{dp}$  by  $\approx 50\%$  (Table 3).  
392 Whilst the CRE plays a role in the sensitivity of the ITCZ to convective mixing (for example,  
393 comparing F1.13PC1.13 and F1.13PC0.57 in Figure 10a), the ITCZ and Hadley circulation are  
394 still sensitive to  $f_{dp}$ . For example, reducing  $f_{dp}$  (F0.57PC1.13) leads to a weakening in the upper  
395 branch of the mean circulation whilst changing the prescribed CRE (F1.13PC0.57) intensifies  
396 the upper branch of the Hadley circulation as the higher  $f_{dp}$  value is associated with a cooler  
397 upper-troposphere, hence, an intensified upper branch of the mean circulation is required for  
398 similar MSE transport (comparing F1.13 in Figure 2b to F0.57PC1.13 and F1.13PC0.57 in Figure  
399 11c and a, respectively). The response of convection to changes in convective mixing is partially  
400 offset by the effect of prescribing the location of the CRE.

401 As in CRE-off simulations, AEI changes in prescribed CRE simulations when varying  $f_{dp}$   
402 are predominantly driven by latent heat flux variations. For example, between F1.13PC1.13 and  
403 F0.57PC1.13, the equatorial latent heat flux reduces whilst the off-equatorial latent heat flux  
404 increases (Figure 12a). These changes are partially offset by changes in the clear-sky radiation,  
405 associated with a decrease in the TOA outgoing longwave radiation, due to an increase in  
406 atmospheric water vapour content. As changes in the ITCZ are associated with AEI changes,  
407 we conclude that the remaining sensitivity of the ITCZ to  $f_{dp}$  in prescribed CRE simulations is

408 associated with latent heat flux variations. In simulations where the prescribed CRE is varied  
 409 but the same  $f_{dp}$  value is used, AEI changes are mostly associated with cloudy-sky radiation  
 410 (Figure 12b, d). However, latent heat flux variations are of the same order of magnitude as when  
 411 varying  $f_{dp}$ . Using the same technique described in section 3c, we conclude that a shallower,  
 412 weaker Hadley circulation is primarily responsible for changes in the MSE transport by the mean  
 413 circulation when reducing  $f_{dp}$  or changing the prescribed CRE from PC1.13 to PC0.57 (not  
 414 shown).

415 F1.13PC0.57 and F0.57PC1.13 have similar, split ITCZs (Figure 10a), yet very different  
 416 AEI profiles (Figure 10b, Figure 11b and d). F0.57PC1.13 highlights that a double ITCZ in  
 417 precipitation does not require a negative  $[AEI]_0$  or an equatorward MSE transport (green and black  
 418 line respectively in Figure 11d), illustrating that a double ITCZ in precipitation is not necessarily  
 419 associated with an equatorward MSE flux at low latitudes. Instead a negative  $[AEI]_0$  is a sufficient  
 420 but not a necessary condition for a double ITCZ in precipitation. Due to local energy conservation  
 421 issues, which are discussed further in section 4, it is challenging to understand F1.13PC0.57,  
 422 which shows a negative  $[AEI]_0$  and a positive equatorial  $\partial_y[\widehat{v}h]$  (Figure 11b), (contradicting (1) as  
 423 steady-state has been reached).

424

#### 425 **4. Discussion**

426 We have analysed aquaplanet simulations with variations to convective mixing to show an  
 427 association between resultant variations in the AEI and characteristics of the ITCZ. Using the AEI  
 428 framework we have shown the importance of the CRE in the sensitivity of the ITCZ to convective  
 429 mixing. In a single ITCZ scenario (F0.85, F1.13 and, F1.70), the CRE is critical in maintaining a  
 430 positive  $[AEI]_0$ . For example, the  $[AEI]_0$  would be negative without the CRE in F1.13 and F1.70,

431 associated with a double ITCZ. Changes in cloudy-sky radiation are the dominant cause of AEI  
432 changes when varying the convective mixing rate, leading to our hypothesis that prescribing the  
433 CRE would remove or reduce the sensitivity of the ITCZ to convective mixing. The fact that the  
434 sensitivity of the ITCZ to  $f_{dp}$  remains in CRE-off and prescribed CRE simulations highlights the  
435 importance of other AEI components, in particular the latent heat flux. All simulations, with the  
436 exception of F0.57PC1.13, are consistent with Bischoff and Schneider (2016): a positive  $[AEI]_0$   
437 is associated with a single ITCZ and a negative  $[AEI]_0$  with a double ITCZ.

438 CRE-off simulations illustrate that the CRE plays a substantial role in the structure and intensity  
439 of the ITCZ. Similar to Harrop and Hartmann (2016), we observe that removing the CRE cools the  
440 tropical upper-troposphere, reducing atmospheric stability and resulting in deep convection over  
441 cooler SSTs. Stronger convection at higher latitudes reduces equatorial moisture convergence and  
442 is associated with a double ITCZ. Removing the CRE also weakens the Hadley circulation which  
443 is associated with a reduced AEI gradient between the tropics and sub-tropics, in agreement  
444 with Popp and Silvers (2017). The sensitivity of the ITCZ to  $f_{dp}$  reduces when removing the  
445 CRE, agreeing with our hypothesis that prescribing the CRE would either remove or reduce  
446 the sensitivity of the ITCZ to convective mixing. Quantifying the reduction in sensitivity of  
447 the ITCZ to  $f_{dp}$  when removing the CRE remains a challenge due to strong dependence on the  
448 chosen metric and range of  $f_{dp}$ . It should also be noted that when removing the CRE other AEI  
449 components change, such that the AEI change is not equal to the total CRE that is removed.

450 In prescribed CRE simulations, ITCZ characteristics are sensitive to both the prescribed CRE  
451 and  $f_{dp}$ , however the sensitivity of the ITCZ to  $f_{dp}$  reduces by  $\approx 50\%$  (Table 3). In prescribed  
452 CRE simulations the response of convection to changes in convective mixing is offset by the effect  
453 of prescribing the location of the CRE. Heating associated with the prescribed CRE is a MSE  
454 source, therefore to increase the MSE exported, convective activity increases. The reduction in

455 sensitivity compliments work by Voigt et al. (2014), who found that prescribing the CRE reduced  
456 the sensitivity of the ITCZ to hemispheric albedo perturbations to a similar degree. Thus, the  
457 role of the CRE in the sensitivity of the ITCZ to both variations in the convection scheme and  
458 boundary forcing appear similar, based on these two studies.

459 In both CRE-off and prescribed CRE simulations, latent heat flux alterations, associated with  
460 circulation changes, are the predominant cause of AEI changes when varying  $f_{dp}$ . Circulation  
461 changes when varying  $f_{dp}$  in CRE-off simulations are not associated with clear-sky flux variations,  
462 consistent with Harrop and Hartmann (2016), which concluded that changes in the clear-sky  
463 radiative cooling do not change the modelled circulation. Mobis and Stevens (2012) highlighted  
464 the importance of surface fluxes in reducing the sensitivity of the ITCZ to the convective  
465 parameterisation scheme when prescribing the wind speeds in the computation of surface fluxes.  
466 Numaguti (1993) and Liu et al. (2010) also concluded that variations in surface evaporation are  
467 associated with the ITCZ structure. We highlight that the sensitivity of the ITCZ to convective  
468 mixing is predominantly associated with the surface fluxes in the absence of cloud feedbacks.

469 As noted earlier in sections 3c and 3d, the balance between the diagnosed AEI and diagnosed  
470  $\partial_y[\widehat{vh}]$ , equation (1), does not hold locally in MetUM. The mean of the maximum absolute  
471 diagnosed imbalance across the tropics amongst simulations is  $13.4 \text{ Wm}^{-2}$ . More importantly,  
472 the diagnosed equatorial energy imbalance ranges from  $6.94 \text{ Wm}^{-2}$  in F0.28NC to  $-20.63 \text{ Wm}^{-2}$   
473 in F1.70 with a mean absolute error of  $9.89 \text{ Wm}^{-2}$ . For all of our simulations apart from  
474 F1.13PC0.57, the sign of the equatorial  $d_y[vh]$  and  $[AEI]_0$  are the same, and therefore using  $[AEI]_0$   
475 as a proxy for the direction of energy transport at low latitudes is still valid. In F1.13PC0.57 the  
476 difference between the diagnosed  $d_y[vh]$  and  $[AEI]$  is  $-16.9 \text{ Wm}^{-2}$ ; the equatorial  $d_y[vh]$  is positive  
477 and  $[AEI]_0$  is slightly negative (Figure 11b). Whilst the local energy imbalance is a concern for  
478 F1.13PC0.57, we argue that in all other simulations the local energy imbalance does not affect

479 our conclusions. There are a number of possible reasons for the localised imbalance of the AEI  
480 budget including: non-conservation associated with the semi-Lagrangian advection scheme in  
481 MetUM; the use of dry and moist density in different components of the MetUM dynamics and  
482 physics; errors in our diagnosis of the MSE budget, for example, not considering density changes  
483 within a timestep; or, using an Eulerian approach for diagnosing the energy transport which is  
484 inconsistent with the semi-Lagrangian advection scheme. It is worth noting that other studies  
485 using the AEI framework have not shown that the MSE energy budget is locally closed, and this  
486 problem may not be unique to our study. Nevertheless, the local energy imbalance has challenged  
487 our interpretation of some simulations, and highlights that future modelling studies using an  
488 atmospheric MSE budget should be cautious.

489 Variations in the CRE when varying  $f_{dp}$  can lead to a negative  $[AEI]_0$  associated with a net  
490 equatorward MSE energy transport at low latitudes. Whilst the predominant response to a negative  
491  $[AEI]_0$  is a double ITCZ associated with equatorward energy transport at low latitudes by the  
492 mean circulation (F0.28, F0.28NC and F0.57NC), F0.57, F0.85NC and F1.13NC have shown  
493 that a net equatorward MSE transport can occur at low latitudes even with a poleward energy  
494 transport by the mean flow at the tropopause. Two mechanisms can lead to this. Firstly, the MSE  
495 flux due to eddies contributes a substantial proportion to the total MSE flux (as seen in Figure  
496 11 12b and d), and this can support equatorward MSE transport. In F0.57, the MSE flux due to  
497 eddies is responsible for a net equatorward energy transport in the deep tropics. This invalidates  
498 the assumption that the energy flux equator is associated with zero MSE transport by the mean  
499 circulation, as in Bischoff and Schneider (2016). This is also supported by the equatorward  
500 displacement of the energy flux equator (from 2 and 4) relative to maximum precipitation in all  
501 simulations except for F0.85NC and F1.70NC (Table 4). The second mechanism (F0.85NC and  
502 F1.13NC) is a change in the MSE transport direction due to a shallower Hadley circulation and a

503 lower MSE in the upper-troposphere (section 3c). These changes reduce the MSE export in the  
504 upper branch of the Hadley circulation, resulting in an equatorward MSE transport by the mean  
505 circulation at low latitudes.

506 In our aquaplanet configuration SSTs are fixed which implies an arbitrary but varying oceanic  
507 heat transport to maintain SSTs given a net surface heat flux imbalance. Thus, our aquaplanet  
508 experiments may be viewed as energetically inconsistent. In Bischoff and Schneider (2014)  
509 and Voigt et al. (2016) ocean heat transport, and hence the net downward flux at the surface, is  
510 fixed, constraining the response of AEI components and potentially reducing the sensitivity of  
511 the ITCZ to model perturbations. In reality the ocean circulation, and thus ocean heat transport,  
512 is sensitive to changes in the surface wind stress. Therefore, both the SST and ocean heat  
513 transport could change in response to tropical circulation changes from variations to  $f_{dp}$  or the  
514 prescribed CRE. Recent work has shown that the ocean circulation plays an important role in  
515 the meridional transport of energy (Green and Marshall 2017), and that sensitivities of the ITCZ  
516 found in atmosphere-only simulations do not necessarily hold in a fully coupled model. For  
517 example, coupling reduces the sensitivity of the ITCZ to an interhemispheric albedo forcing (e.g.  
518 comparing Kay et al. (2016) and Hawcroft et al. (2017) to Voigt et al. (2014)). The radiative  
519 effect of clouds on the surface and Ekman heat transport associated with a single ITCZ would be  
520 expected to reduce the equatorial SST gradient, which would promote a double ITCZ (Numaguti  
521 1995; Mobis and Stevens 2012) and may reduce the sensitivity of the ITCZ to convective mixing.  
522 Coupled simulations with an interactive ocean are required to further investigate the sensitivity of  
523 the ITCZ to the CRE and convective mixing.

524

## 525 **5. Conclusions**

526 The double ITCZ bias is a leading systematic error across a hierarchy of models (Li and Xie  
527 2014; Oueslati and Bellon 2015). Inter-model variability in the ITCZ structure persists even  
528 in a highly-idealised framework such as an aquaplanet with prescribed SSTs (Blackburn et al.  
529 2013). This study confirms and extends previous research that variations in the convective  
530 parameterisation scheme and convective mixing can alter the ITCZ (Figure 1a; Hess et al. 1993;  
531 Numaguti 1995; Chao and Chen 2004; Liu et al. 2010; Mobis and Stevens 2012). Higher  
532 convective mixing rates are associated with a single ITCZ whilst lower rates are associated with a  
533 double ITCZ. As the convective mixing rate reduces, convection at higher latitudes strengthens,  
534 decreasing equatorward low-level winds at low latitudes, promoting a double ITCZ structure.  
535 The sensitivity of the ITCZ to convective mixing is associated with AEI changes, predominantly  
536 caused by CRE variations. For example, the CRE plays an important role in maintaining a  
537 positive equatorial AEI, and is therefore associated with a single ITCZ structure (consistent with  
538 Harrop and Hartmann (2016) and Bischoff and Schneider (2016)'s framework). When removing  
539 the CRE, the response of the ITCZ depends on the convective mixing rate. At low convective  
540 mixing rates, where a double ITCZ is simulated with the CRE, precipitation bands shift poleward.  
541 At high convective mixing rates the ITCZ broadens, whilst at certain convective mixing rates the  
542 ITCZ structure changes from single to double. Quantifying whether the sensitivity of the ITCZ  
543 to convective mixing reduces when removing the CRE is challenging, as the sensitivity depends  
544 on the range of convective mixing rates and the chosen metric. Prescribing the CRE reduces  
545 the sensitivity of the ITCZ to convective mixing by  $\approx 50\%$ . When removing or prescribing the  
546 CRE other AEI components, in particular the latent heat flux, play a role in the sensitivity of  
547 the ITCZ to convective mixing. Hence, simulations where the ocean heat transport is fixed,

548 thereby constraining surface fluxes, may underestimate the sensitivity of the ITCZ to changes  
549 in model formulation. We have also shown two mechanisms responsible for a net equatorward  
550 MSE transport even with no equatorial subsidence: MSE transport by eddies; and a reduced MSE  
551 export in the upper branch of the mean circulation due to a shallower Hadley circulation. These  
552 mechanisms highlight that caution should be taken when associating changes in the AEI to the  
553 ITCZ structure.

554

555 *Acknowledgments.* JT is funded by the Natural Environment Research Council (NERC) via the  
556 SCENARIO Doctoral Training Partnership (NE/L002566/1) at the University of Reading. SJW  
557 was supported by the National Centre for Atmospheric Science, a NERC collaborative centre  
558 under contract R8/H12/83/001. NPK was supported by an Independent Research Fellowship from  
559 the NERC (NE/LO10976/1). The data used in this publication is available on request from the  
560 lead author.

561 We would like to thank Aiko Voigt and two anonymous reviewers for comments which  
562 substantially improved this paper.

563

## 564 **References**

565 Adam, O., T. Bischoff, and T. Schneider, 2016: Seasonal and interannual variations of the energy  
566 flux equator and ITCZ. Part I: Zonally averaged ITCZ position. *J. Climate.*, **29** (9), 3219–3230.

567 Allan, R. P., 2011: Combining satellite data and models to estimate cloud radiative effect at the  
568 surface and in the atmosphere. *Meteorological Applications*, **18** (3), 324–333, doi:10.1002/met.  
569 285.

- 570 Bischoff, T., and T. Schneider, 2014: Energetic Constraints on the Position of the Intertropical  
571 Convergence Zone. *J. Climate.*, **27**, 4937–4951, doi:10.1175/JCLI-D-13-00650.1.
- 572 Bischoff, T., and T. Schneider, 2016: The Equatorial Energy Balance, ITCZ Position, and Double-  
573 ITCZ Bifurcations. *J. Climate.*, **29** (8), 2997–3013, and Corrigendum, 29(19), 7167–7167, doi:  
574 10.1175/JCLI-D-15-0328.1.
- 575 Blackburn, M., and Coauthors, 2013: The aqua-planet experiment (APE): Control SST simulation.  
576 *J. Meteor. Soc. Japan. Ser. II*, **91**, 17–56.
- 577 Bush, S., A. Turner, S. Woolnough, G. Martin, and N. Klingaman, 2015: The effect of increased  
578 convective entrainment on Asian monsoon biases in the MetUM general circulation model.  
579 *Quart. J. Roy. Meteor. Soc.*, 311–326, doi:{10.1002/qj.2371}.
- 580 Chao, W. C., and B. Chen, 2004: Single and double ITCZ in an aqua-planet model with con-  
581 stant sea surface temperature and solar angle. *Climate Dyn.*, **22** (4), 447–459, doi:10.1007/  
582 s00382-003-0387-4.
- 583 Chikira, M., 2010: A cumulus parameterization with state-dependent entrainment rate. Part II:  
584 Impact on climatology in a general circulation model. *J. Atmos. Sci.*, **67** (7), 2194–2211, doi:  
585 10.1175/2010JAS3317.1.
- 586 Crueger, T., and B. Stevens, 2015: The effect of atmospheric radiative heating by clouds  
587 on the Madden-Julian Oscillation. *J. Adv. Model. Earth Syst.*, **7** (2), 854–864, doi:10.1002/  
588 2015MS000434.
- 589 Derbyshire, S. H., I. Beau, P. Bechtold, J.-Y. Grandpeix, J.-M. Piriou, J.-L. Redelsperger, and  
590 P. M. M. Soares, 2004: Sensitivity of moist convection to environmental humidity. *Quart. J.*  
591 *Roy. Meteor. Soc.*, **130** (604), 3055–3079, doi:10.1256/qj.03.130.

592 Donohoe, A., J. Marshall, D. Ferreira, and D. Mcgee, 2013: The relationship between ITCZ  
593 location and cross-equatorial atmospheric heat transport: From the seasonal cycle to the last  
594 glacial maximum. *Amer. Meteor. Soc.*, 3597–3618, doi:10.1175/JCLIM-D-12-00467.1.

595 Fermepin, S., and S. Bony, 2014: Influence of low-cloud radiative effects on tropical circulation  
596 and precipitation. *J. Adv. Model. Earth Syst.*, **6** (3), 513–526, doi:10.1002/2013MS000288.

597 Frierson, D., and Y. Hwang, 2012: Extratropical Influence on ITCZ Shifts in Slab Ocean Simula-  
598 tions of Global Warming. *J. Climate.*, 720–733, doi:{10.1175/JCLI-D-11-00116.1}.

599 Frierson, D. M. W., 2007: The dynamics of idealized convection schemes and their effect on the  
600 zonally averaged tropical circulation. *J. Atmos. Sci.*, **64** (6), 1959–1976, doi:10.1175/JAS3935.  
601 1, <http://dx.doi.org/10.1175/JAS3935.1>.

602 Fritsch, J. M., and C. F. Chappell, 1980: Numerical prediction of convectively driven mesoscale  
603 pressure systems. Part I: Convective parameterization. *J. Atmos. Sci.*, **37** (8), 1722–1733, doi:  
604 10.1175/1520-0469(1980)037<1722:NPOCDM>2.0.CO;2.

605 Green, B., and J. Marshall, 2017: Coupling of trade winds with ocean circulation damps ITCZ  
606 shifts. *J. Climate.*, **30** (12), 4395–4411.

607 Gregory, D., and P. Rowntree, 1990: A mass flux convection scheme with representation of cloud  
608 ensemble characteristics and stability-dependent closure. *Mon. Weather Rev.*, **118** (7), 1483–  
609 1506.

610 Harrop, B., and D. Hartmann, 2016: The role of cloud radiative heating in determining the lo-  
611 cation of the ITCZ in aquaplanet simulations. *Amer. Meteor. Soc.*, 2714–2763, doi:{10.1175/  
612 JCLI-D-15-0521.1}.

- 613 Hawcroft, M., J. M. Haywood, M. Collins, A. Jones, A. C. Jones, and G. Stephens, 2017: Southern  
614 ocean albedo, inter-hemispheric energy transports and the double ITCZ: global impacts of biases  
615 in a coupled model. *Climate Dynamics*, **48** (7), 2279–2295, doi:10.1007/s00382-016-3205-5.
- 616 Hess, P. G., D. S. Battisti, and P. J. Rasch, 1993: Maintenance of the Intertropical Convergence  
617 Zones and the large-scale tropical circulation on a water-covered earth. *J. Atmos. Sci.*, **50** (5),  
618 691–713, doi:10.1175/1520-0469(1993)050<0691:MOTICZ>2.0.CO;2.
- 619 Kang, S., I. Held, D. Frierson, and Z. Ming, 2008: The Response of the ITCZ to Extratropical  
620 Thermal Forcing: Idealized Slab-Ocean Experiments with a GCM. *Amer. Meteor. Soc.*, 3521–  
621 3532, doi:{10.1175/2007JCLI2146.1}.
- 622 Kay, J. E., C. Wall, V. Yettella, B. Medeiros, C. Hannay, P. Caldwell, and C. Bitz, 2016: Global  
623 climate impacts of fixing the southern ocean shortwave radiation bias in the community earth  
624 system model (CESM). *J. Climate*, **29** (12), 4617–4636, doi:10.1175/JCLI-D-15-0358.1.
- 625 Li, G., and S.-P. Xie, 2014: Tropical biases in CMIP5 multimodel ensemble: The excessive  
626 equatorial pacific cold tongue and double ITCZ problems. *J. Climate*, **27** (4), 1765–1780, doi:  
627 10.1175/JCLI-D-13-00337.1.
- 628 Li, Y., D. W. J. Thompson, and S. Bony, 2015: The influence of atmospheric cloud radiative  
629 effects on the large-scale atmospheric circulation. *J. Climate.*, **28** (18), 7263–7278, doi:10.1175/  
630 JCLI-D-14-00825.1.
- 631 Lin, J., 2007: The Double-ITCZ Problem in IPCC AR4 Coupled GCMs: Ocean-Atmosphere  
632 Feedback Analysis. *Amer. Meteor. Soc.*, 4497–4525, doi:{10.1175/JCLI4272.1}.

- 633 Liu, Y., L. Guo, G. Wu, and Z. Wang, 2010: Sensitivity of ITCZ configuration to cumu-  
634 lus convective parameterizations on an aqua planet. *Climate Dyn.*, **34** (2), 223–240, doi:  
635 10.1007/s00382-009-0652-2.
- 636 Mobis, B., and B. Stevens, 2012: Factors controlling the position of the Intertropical Convergence  
637 Zone on an aquaplanet. *J. Adv. Model. Earth Syst.*, **4** (4), doi:10.1029/2012MS000199, m00A04.
- 638 Neale, R., and B. Hoskins, 2001: A standard test for AGCMs including their physical parametriza-  
639 tions: I: The proposal. *Atmos. Sci. Letters*, doi:{10.1006/asle.2000.0019}.
- 640 Neelin, J. D., and I. M. Held, 1987: Modeling tropical convergence based on the moist static  
641 energy budget. *Mon. Weather Rev.*, **115** (1), 3–12.
- 642 Nolan, D., S. Tulich, and J. Blanco, 2016: ITCZ structure as determined by parameterized versus  
643 explicit convection in aquachannel and aquapatch simulations. *J. Adv. Model. Earth Syst.*, **8**,  
644 1–28, doi:{10.1002/2015MS000560}.
- 645 Nordeng, T. E., 1994: *Extended versions of the convective parametrization scheme at ECMWF*  
646 *and their impact on the mean and transient activity of the model in the tropics*. European Centre  
647 for Medium-Range Weather Forecasts.
- 648 Numaguti, A., 1993: Dynamics and energy balance of the Hadley circulation and the tropical  
649 precipitation zones: Significance of the distribution of evaporation. *J. Atmos. Sci.*, **50** (13),  
650 1874–1887, doi:10.1175/1520-0469(1993)050<1874:DAEBOT>2.0.CO;2.
- 651 Numaguti, A., 1995: Dynamics and energy balance of the Hadley circulation and the tropical  
652 precipitation zones. Part II: Sensitivity to meridional SST distribution. *J. Atmos. Sci.*, **52** (8),  
653 1128–1141, doi:10.1175/1520-0469(1995)052<1128:DAEBOT>2.0.CO;2.

- 654 Oueslati, B., and G. Bellon, 2013: Convective entrainment and large-scale organization of tropical  
655 precipitation: Sensitivity of the CNRM-CM5 hierarchy of models. *J. Climate.*, **26** (9), 2931–  
656 2946, doi:10.1175/JCLI-D-12-00314.1.
- 657 Oueslati, B., and G. Bellon, 2015: The double ITCZ bias in CMIP5 models: interaction be-  
658 tween SST, large-scale circulation and precipitation. *Climate Dyn.*, **44** (3), 585–607, doi:  
659 10.1007/s00382-015-2468-6.
- 660 Popp, M., and L. G. Silvers, 2017: Double and single ITCZs with and without clouds. *Journal of*  
661 *Climate*, **30** (22), 9147–9166.
- 662 Schneider, T., T. Bischoff, and G. Haug, 2014: Migrations and dynamics of the Intertropical  
663 Convergence Zone. **513**, 45–53, doi:10.1038/nature13636.
- 664 Slingo, A., and J. M. Slingo, 1988: The response of a general circulation model to cloud longwave  
665 radiative forcing. I: Introduction and initial experiments. *Quart. J. Roy. Meteor. Soc.*, **114** (482),  
666 1027–1062, doi:10.1002/qj.49711448209.
- 667 Sobel, A. H., J. Nilsson, and L. M. Polvani, 2001: The weak temperature gradient  
668 approximation and balanced tropical moisture waves. *Journal of the Atmospheric Sci-*  
669 *ences*, **58** (23), 3650–3665, doi:10.1175/1520-0469(2001)058<3650:TWTGAA>2.0.CO;2,  
670 URL [https://doi.org/10.1175/1520-0469\(2001\)058<3650:TWTGAA>2.0.CO;2](https://doi.org/10.1175/1520-0469(2001)058<3650:TWTGAA>2.0.CO;2), [https://doi.org/](https://doi.org/10.1175/1520-0469(2001)058<3650:TWTGAA>2.0.CO;2)  
671 [10.1175/1520-0469\(2001\)058<3650:TWTGAA>2.0.CO;2](https://doi.org/10.1175/1520-0469(2001)058<3650:TWTGAA>2.0.CO;2).
- 672 Terray, L., 1998: Sensitivity of climate drift to atmospheric physical parameterizations in a cou-  
673 pled ocean-atmosphere general circulation model. *J. Climate.*, **11**, 1633–1658, doi:10.1175/  
674 1520-0442(1998)011<1633:SOCDTA>2.0.CO;2.

- 675 Tiedtke, M., 1989: A comprehensive mass flux scheme for cumulus parameterization in large-  
676 scale models. *Mon. Weather Rev.*, **117** (8), 1779–1800.
- 677 Voigt, A., S. Bony, J.-L. Dufresne, and B. Stevens, 2014: The radiative impact of clouds on the  
678 shift of the Intertropical Convergence Zone. *Geophysical Research Letters*, **41** (12), 4308–4315,  
679 doi:10.1002/2014GL060354, URL <http://dx.doi.org/10.1002/2014GL060354>.
- 680 Voigt, A., and Coauthors, 2016: The tropical rain belts with an annual cycle and a continent model  
681 intercomparison project: TRACMIP. *Journal of Advances in Modeling Earth Systems*, **8** (4),  
682 1868–1891, doi:10.1002/2016MS000748, URL <http://dx.doi.org/10.1002/2016MS000748>.
- 683 Walters, D., and Coauthors, 2017: The Met Office Unified Model Global Atmosphere 6.0/6.1  
684 and JULES Global Land 6.0/6.1 configurations. *Geosci. Model Dev. Discuss.*, **2016**, 1–52, doi:  
685 10.5194/gmd-2016-194, URL <http://www.geosci-model-dev-discuss.net/gmd-2016-194/>.
- 686 Wang, Y., L. Zhou, and K. Hamilton, 2007: Effect of convective entrainment/detrainment on the  
687 simulation of the tropical precipitation diurnal cycle. *Mon. Weather Rev.*, **135** (2), 567–585, doi:  
688 10.1175/MWR3308.1, URL [http://dx.doi.org/10.1175/](http://dx.doi.org/10.1175/MWR3308.1)  
689 [MWR3308.1](http://dx.doi.org/10.1175/MWR3308.1).

690 **LIST OF TABLES**

691 **Table 1.** Simulations varying  $f_{dp}$  with cloud-radiation interactions on (CRE-on) and off  
692 (CRE-off). F1.13 is the default integration for GA6.0. . . . . 34

693 **Table 2.** Simulations with a prescribed climatology of the CRE diurnal cycle. PC1.13  
694 and PC0.57 represent the prescribed CRE diurnal cycle from a one-year simu-  
695 lation where  $f_{dp}$  equals 1.13 or 0.57 (respectively). . . . . 35

696 **Table 3.** Root mean squared difference for tropical precipitation and mass meridional  
697 streamfunction between two simulations. Tropical domain defined as 30°N  
698 to 30°S. Percentage value is the percentage reduction compared to F0.57 and  
699 F1.13. . . . . 36

700 **Table 4.**  $AEI_0$ , location of ITCZ and approximate energy flux equator ( $\delta$ ) using equation  
701 2 or 4 in each simulation. A single/double ITCZ is assumed when  $AEI_0$  is  
702 positive/negative, respectively. Not applicable (N/A) occurs when  $AEI_0$  and  
703  $\partial_{yy}([AEI])_0$  are both negative and therefore the square root of  $-\frac{6([AEI])_0}{\partial_{yy}([AEI])_0}$  has  
704 an imaginary component. . . . . 37

705 TABLE 1. Simulations varying  $f_{dp}$  with cloud-radiation interactions on (CRE-on) and off (CRE-off). F1.13 is  
 706 the default integration for GA6.0.

$f_{dp}$	CRE-on	CRE-off
0.28	F0.28	F0.28NC
0.57	F0.57	F0.57NC
0.85	F0.85	F0.85NC
1.13	F1.13	F1.13NC
1.70	F1.70	F1.70NC

707 TABLE 2. Simulations with a prescribed climatology of the CRE diurnal cycle. PC1.13 and PC0.57 represent  
 708 the prescribed CRE diurnal cycle from a one-year simulation where  $f_{dp}$  equals 1.13 or 0.57 (respectively).

$f_{dp}$	PC1.13	PC0.57
1.13	F1.13PC1.13	F1.13PC0.57
0.57	F0.57PC1.13	F0.57PC0.57

709 TABLE 3. Root mean squared difference for tropical precipitation and mass meridional streamfunction be-  
 710 tween two simulations. Tropical domain defined as 30°N to 30°S. Percentage value is the percentage reduction  
 711 compared to F0.57 and F1.13.

Simulations	Precipitation (mm day <sup>-1</sup> )	Mass Meridional Streamfunction ( $\times 10^{10}$ kg s <sup>-1</sup> )
F0.57 & F1.13	2.84	1.78
F0.57PC1.13 & F1.13PC1.13	1.18 (58%)	0.67 (62%)
F0.57PC0.57 & F1.13PC0.57	1.65 (42%)	0.96 (46%)

712 TABLE 4.  $AEI_0$ , location of ITCZ and approximate energy flux equator ( $\delta$ ) using equation 2 or 4 in each  
713 simulation. A single/double ITCZ is assumed when  $AEI_0$  is positive/negative, respectively. Not applicable  
714 (N/A) occurs when  $AEI_0$  and  $\partial_{yy}([AEI])_0$  are both negative and therefore the square root of  $-\frac{6([AEI])_0}{\partial_{yy}([AEI])_0}$  has an  
715 imaginary component.

Simulation	$AEI_0$ ( $\text{W m}^{-2}$ )	ITCZ location ( $^\circ$ )	Energy Flux Equator ( $\delta$ ) location ( $^\circ$ )
F0.28	-18.1	8.13/8.13	6.85/-7.06
F0.57	-5.9	4.38/-4.38	0.84/-2.87
F0.85	33.4	1.88	-0.41
F1.13	36.7	0.63	0.22
F1.70	33.7	0.63	0.30
F0.28NC	-4.9	9.38/-9.38	N/A
F0.57NC	-12.2	8.13/-8.13	N/A
F0.85NC	-18.3	6.88/-5.63	6.48/-6.80
F1.13NC	-5.9	4.38/-4.38	3.21/-3.58
F1.70NC	2.0	1.88	2.73
F1.13PC1.13	33.6	0.63	0.16
F1.13PC0.57	-1.7	3.13/-3.13	0.19/-1.75
F0.57PC1.13	20.6	3.13	-0.12
F0.57PC0.57	-14.2	4.38/-4.38	2.70/-2.64

716 **LIST OF FIGURES**

717 **Fig. 1.** Zonal-, time-mean (a) precipitation rates ( $\text{mm day}^{-1}$ ) and (b) AEI ( $\text{W m}^{-2}$ ) in simulations  
718 where  $f_{dp}$  is varied. . . . . 40

719 **Fig. 2.** Zonal-, time-mean mass meridional streamfunction ( $\text{kg s}^{-1}$ ) (lined contours) and vertical  
720 wind speed ( $\text{m s}^{-1}$ ) (filled contours). Lined contours are in intervals of  $5 \times 10^{10}$ , with  
721 dashed contours representing negative values. Dotted contour is zero value. (a): F1.70,  
722 (b): F1.13, (c): F0.85, (d): F0.57, (e): F0.28. Maximum value of the mass meridional  
723 streamfunction printed in top right-hand corner of each subplot. . . . . 41

724 **Fig. 3.** Zonal, time-mean AEI components ( $\text{W m}^{-2}$ ). (b): F1.13 and (a),(c)-(e): Change in AEI  
725 components compared to F1.13 for (a) F1.70; (c) F0.85, (d) F0.57, (e) F0.28. Red line is  
726 the clear-sky component, blue line is the cloudy-sky component. Green and orange lines  
727 represent the sensible and latent heat flux, respectively, and the black line is the total change  
728 in AEI. Note, (a) and (c) have axis limits  $-15$  and  $15 \text{ W m}^{-2}$ , whilst (d) and (e) have limits  
729  $-75$  and  $75 \text{ W m}^{-2}$ . . . . . 42

730 **Fig. 4.** Zonal-, time-mean (a) precipitation rates ( $\text{mm day}^{-1}$ ) and (b) AEI ( $\text{W m}^{-2}$ ) in CRE-off  
731 simulations where  $f_{dp}$  is varied. . . . . 43

732 **Fig. 5.** Zonal-, time-mean mass meridional streamfunction ( $\text{kg s}^{-1}$ ) (lined contours) and vertical  
733 wind speed ( $\text{m s}^{-1}$ ) (filled contours). Lined contours are in intervals of  $5 \times 10^{10}$ , with  
734 dashed contours representing negative values. Dotted contour is zero value. (a) F1.70NC, (b)  
735 F1.13NC, (c) F0.85NC, (d) F0.57NC, (e) F0.28NC. Maximum value of the mass meridional  
736 streamfunction printed in top right-hand corner of each subplot. . . . . 44

737 **Fig. 6.** Zonal, time-mean AEI components ( $\text{W m}^{-2}$ ). (b) F1.13NC (a),(c)-(e): Change in AEI com-  
738 ponents compared to F1.13NC for (a) F1.70NC; (c) F0.85NC, (d) F0.57NC, (e) F0.28NC  
739 and (f): Change in AEI components when removing cloud-radiation interactions at  $f_{dp}$   
740 equals 1.13 (F1.13NC - F1.13). Note, (a) and (c) have axis limits  $-20$  and  $20 \text{ W m}^{-2}$  whilst  
741 (d)-(f) have limits  $-80$  and  $80 \text{ W m}^{-2}$ . . . . . 45

742 **Fig. 7.** Diagnostics for determining the sensitivity of the ITCZ to  $f_{dp}$  in CRE-on (green) and CRE-  
743 off (blue) simulations. Top (a): Latitude of maximum precipitation ( $^\circ$ ), bottom (b): Precipi-  
744 tation rate at ITCZ ( $\text{mm day}^{-1}$ ). Four regression lines are plotted in each subplot. Solid lines  
745 where  $0.28 \leq f_{dp} \leq 1.13$  and dashed lines where  $f_{dp} \leq 1.70$ . The slope of each regression  
746 line is printed in the legend. First value where  $0.28 \leq f_{dp} \leq 1.13$  and second value where  
747  $f_{dp} \leq 1.70$ . . . . . 46

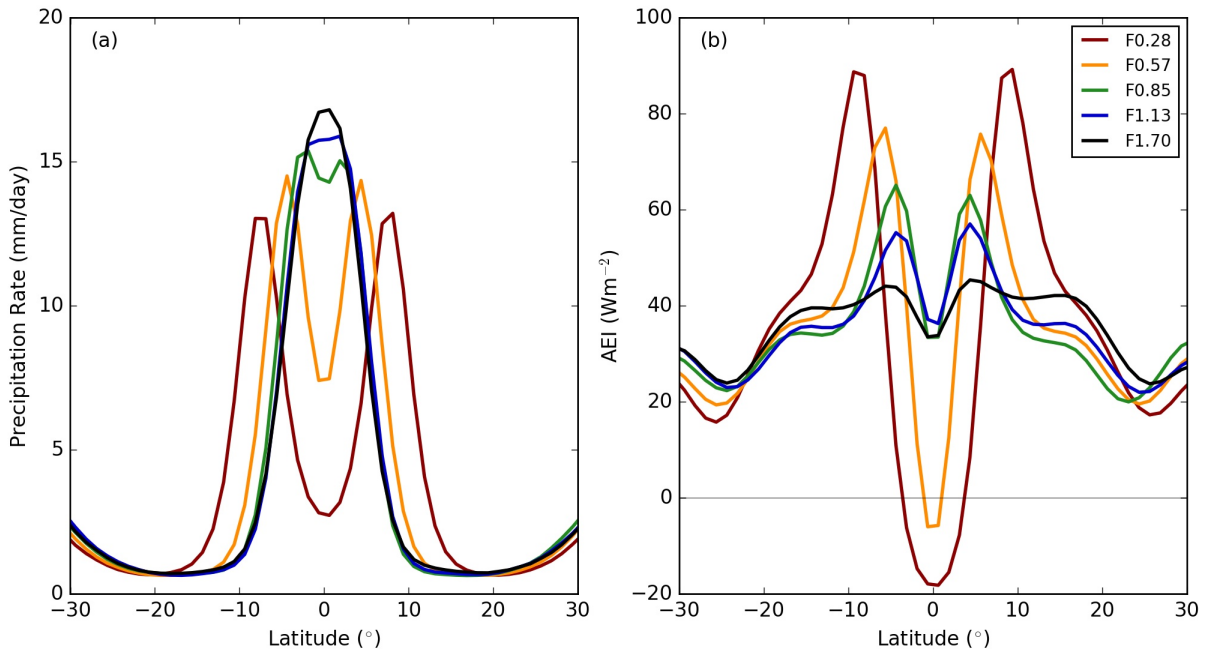
748 **Fig. 8.** Zonal-, time-mean cloud fraction against temperature (K) at latitude of maximum precipi-  
749 tation. Left (a): CRE-on simulations, right (b): CRE-off simulations. Printed in legend, the  
750 tropical-domain average CRE ( $\text{W m}^{-2}$ ) for CRE-on simulations. . . . . 47

751 **Fig. 9.** Top row: (a) and (b): Meridional mass flux ( $\text{kg m}^{-1} \text{ s}^{-1}$ ) in F1.13NC and F1.13 respec-  
752 tively, (c) and (d): Change in meridional mass flux due to change in circulation strength and  
753 change in meridional wind, respectively. Bottom row: Components of MSE flux change ( $\text{W}$   
754  $\text{m}^{-1}$ ), equation (10), due to (e), circulation intensity changes  $\alpha V_c h_c$ , (f), changes in circula-  
755 tion structure  $V_r h_c$ , (g), MSE profile changes  $V_c h_p$ , and, (h), MSE changes correlated with  
756 changes in circulation structure and strength ( $\alpha V_c + V_r$ )  $h_p$ . Analysis explained in Section 3c. . . . . 48

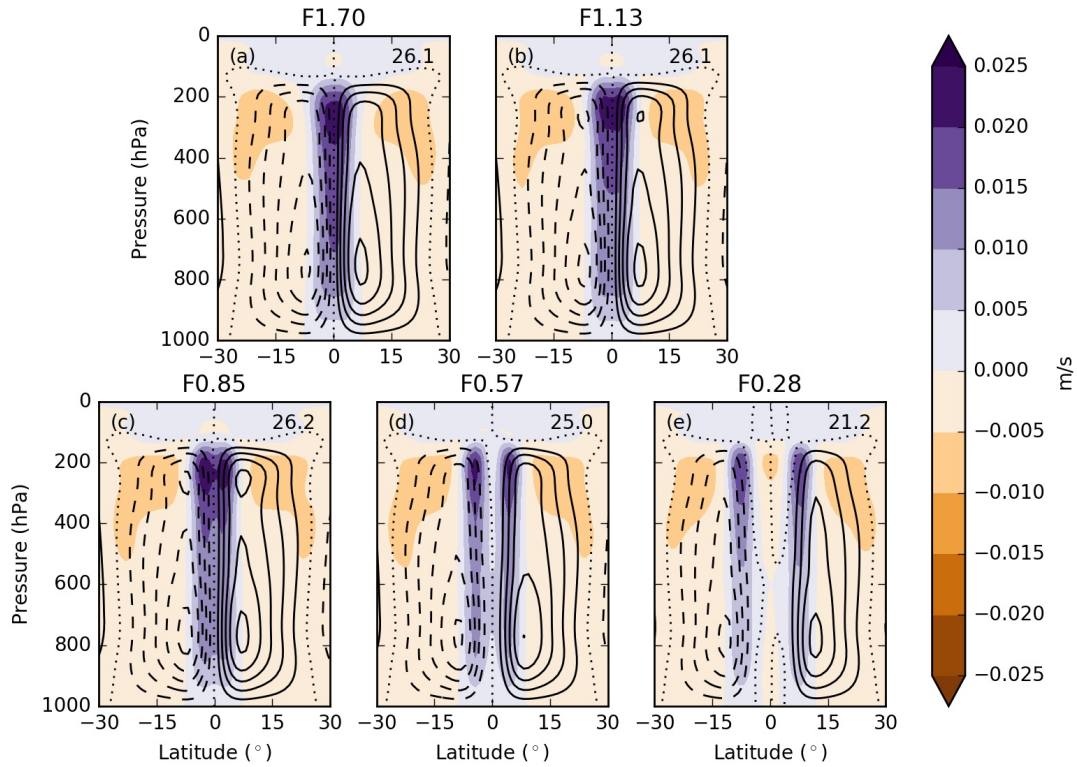
757 **Fig. 10.** Zonal-, time-mean (a) precipitation rates ( $\text{mm day}^{-1}$ ) and (b) AEI ( $\text{W m}^{-2}$ ) in simulations  
758 with a prescribed CRE. . . . . 49

759 **Fig. 11.** Left: Zonal-, time-mean mass meridional streamfunction ( $\text{kg s}^{-1}$ ) (lined contours) and ver-  
760 tical wind speed ( $\text{m s}^{-1}$ ) (filled contours) for (a) F1.13PC0.57 and (c) F0.57PC1.13. Lined  
761 contours are in intervals of  $5 \times 10^{10}$ , with dashed contours representing negative values.  
762 Dotted contour is zero value and maximum value of the mass meridional streamfunction  
763 printed in top right-hand corner of each subplot. Right: Divergence of the MSE flux ( $\text{W}$   
764  $\text{m}^{-2}$ ) and AEI for (b) F1.13PC0.57 and (d) F0.57PC1.13. Solid black line - Divergence of  
765 total MSE flux  $\partial_y[\widehat{vh}]$ , red dotted line - MSE flux due to mean circulation  $\partial_y[\widehat{v}][\widehat{h}]$ , blue line  
766 -  $\partial_y[\widehat{vh}] - \partial_y[\widehat{v}][\widehat{h}]$ , green line -  $[AEI]$ . . . . . 50

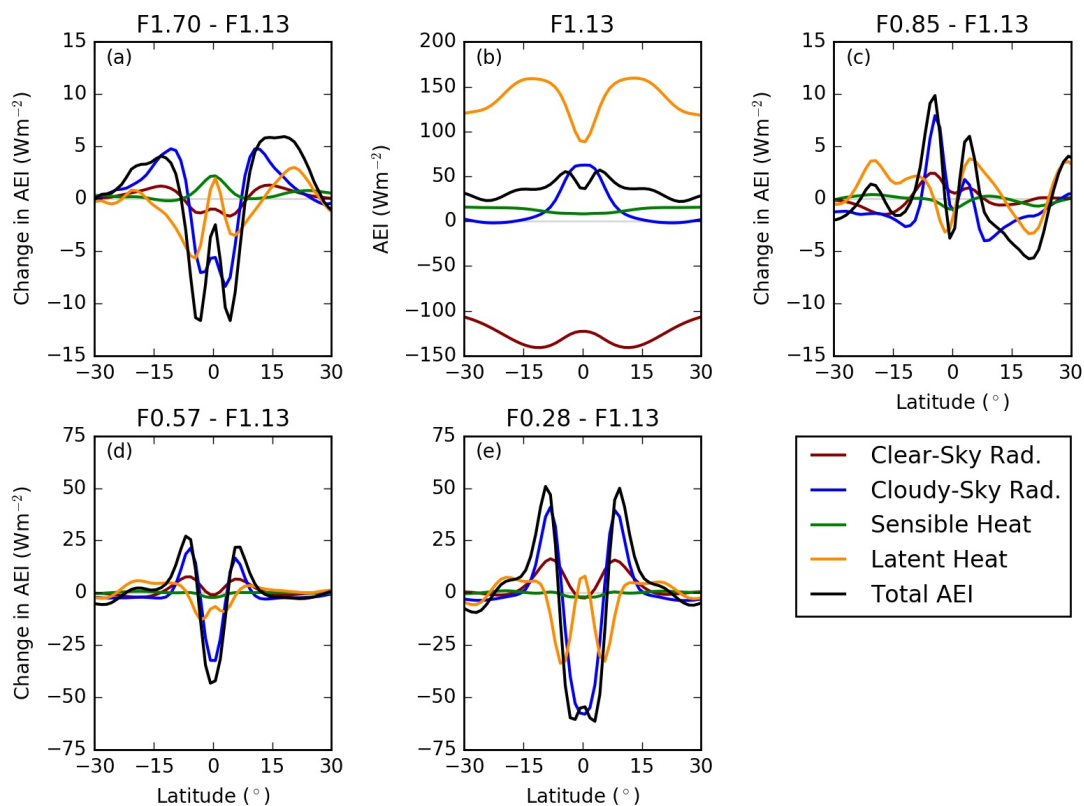
767 **Fig. 12.** Changes in zonal-, time-mean AEI contributions ( $\text{W m}^{-2}$ ) for prescribed CRE simulations.  
768 Comparison of simulations with same  $f_{dp}$  constant (a, c) have y-axis limits of -15 to 15  $\text{W}$   
769  $\text{m}^{-2}$ , whilst those with a different prescribed CRE (b, d) have y-axis limits -45 to 45  $\text{W m}^{-2}$ . . . . . 51



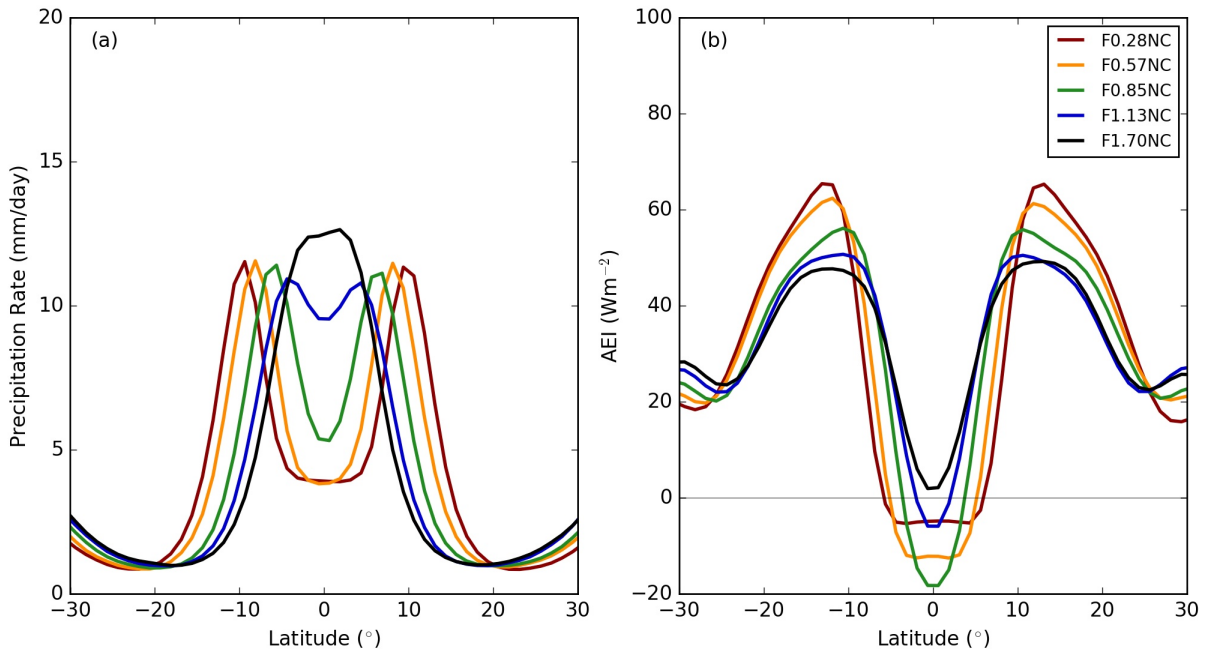
770 FIG. 1. Zonal-, time-mean (a) precipitation rates ( $mm day^{-1}$ ) and (b) AEI ( $W m^{-2}$ ) in simulations where  $f_{dp}$   
 771 is varied.



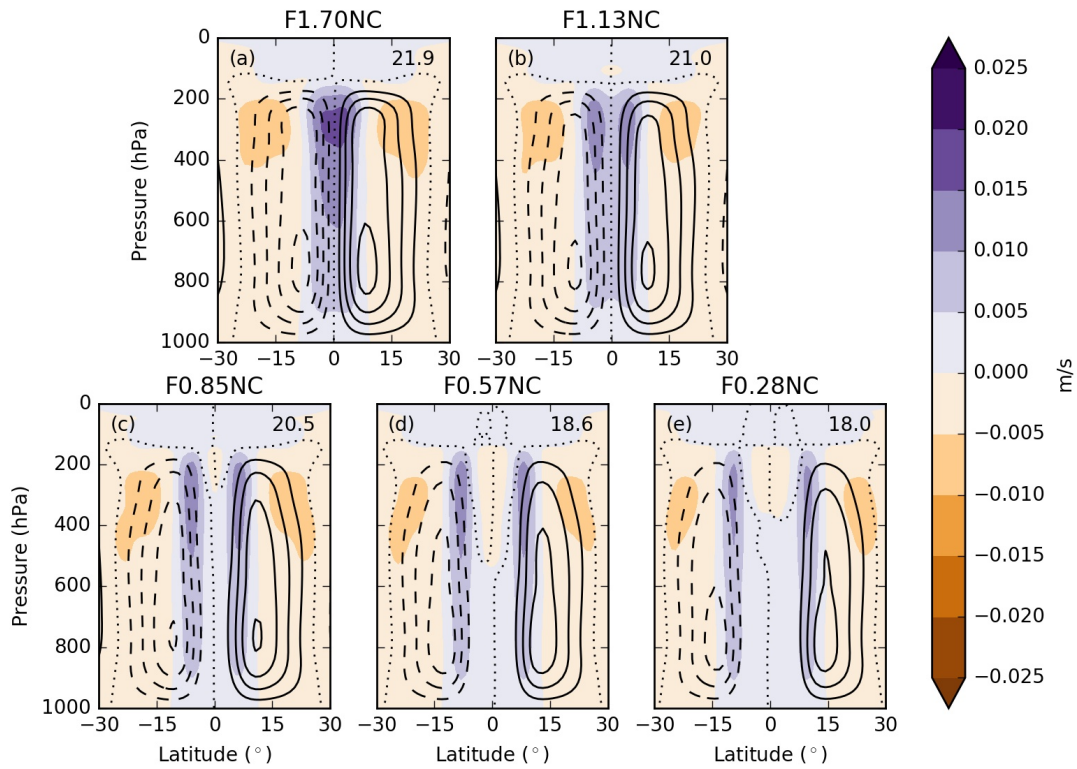
772 FIG. 2. Zonal-, time-mean mass meridional streamfunction ( $\text{kg s}^{-1}$ ) (lined contours) and vertical wind speed  
 773 ( $\text{m s}^{-1}$ ) (filled contours). Lined contours are in intervals of  $5 \times 10^{10}$ , with dashed contours representing negative  
 774 values. Dotted contour is zero value. (a): F1.70, (b): F1.13, (c): F0.85, (d): F0.57, (e): F0.28. Maximum value  
 775 of the mass meridional streamfunction printed in top right-hand corner of each subplot.



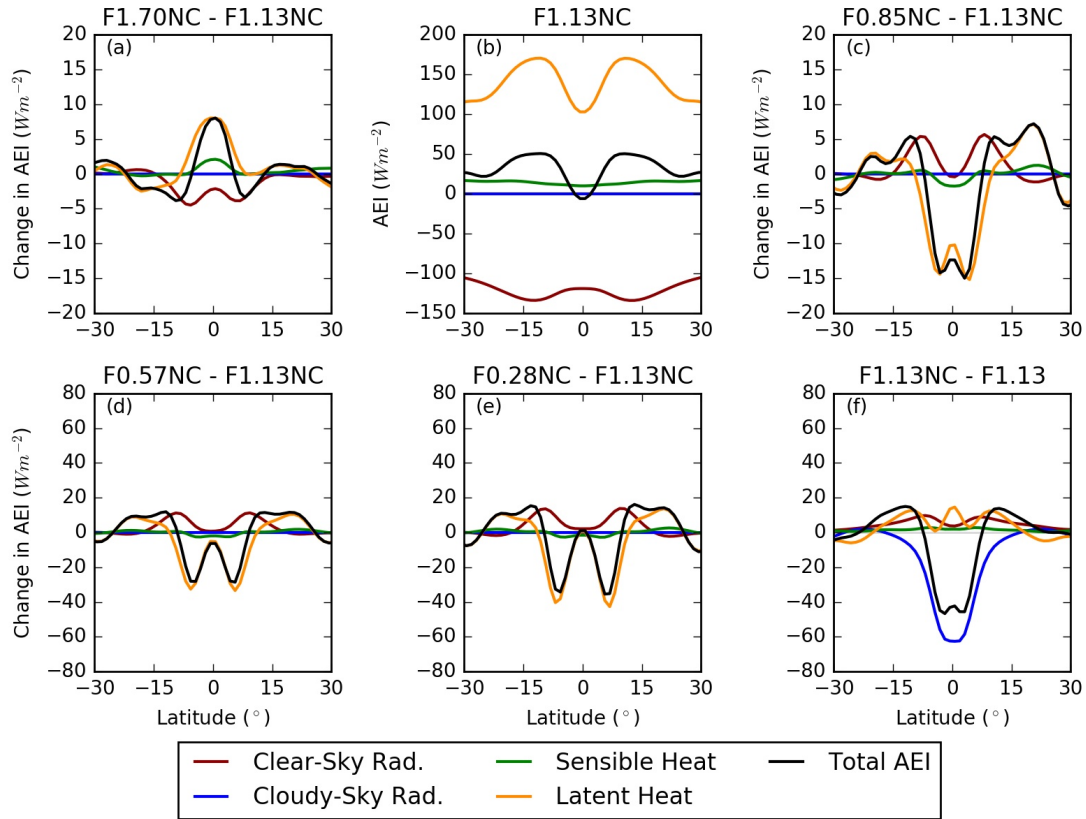
776 FIG. 3. Zonal, time-mean AEI components ( $\text{W m}^{-2}$ ). (b): F1.13 and (a),(c)-(e): Change in AEI components  
 777 compared to F1.13 for (a) F1.70; (c) F0.85, (d) F0.57, (e) F0.28. Red line is the clear-sky component, blue line  
 778 is the cloudy-sky component. Green and orange lines represent the sensible and latent heat flux, respectively,  
 779 and the black line is the total change in AEI. Note, (a) and (c) have axis limits  $-15$  and  $15 \text{ W m}^{-2}$ , whilst (d) and  
 780 (e) have limits  $-75$  and  $75 \text{ W m}^{-2}$ .



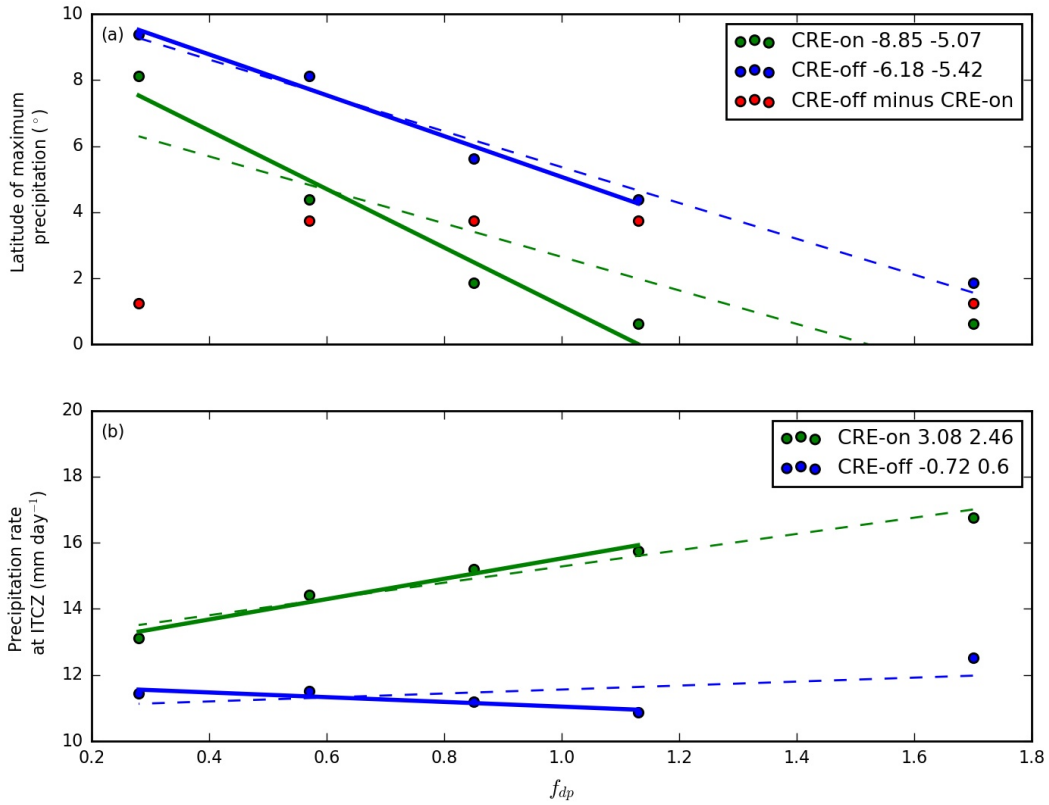
781 FIG. 4. Zonal-, time-mean (a) precipitation rates ( $mm day^{-1}$ ) and (b) AEI ( $W m^{-2}$ ) in CRE-off simulations  
 782 where  $f_{dp}$  is varied.



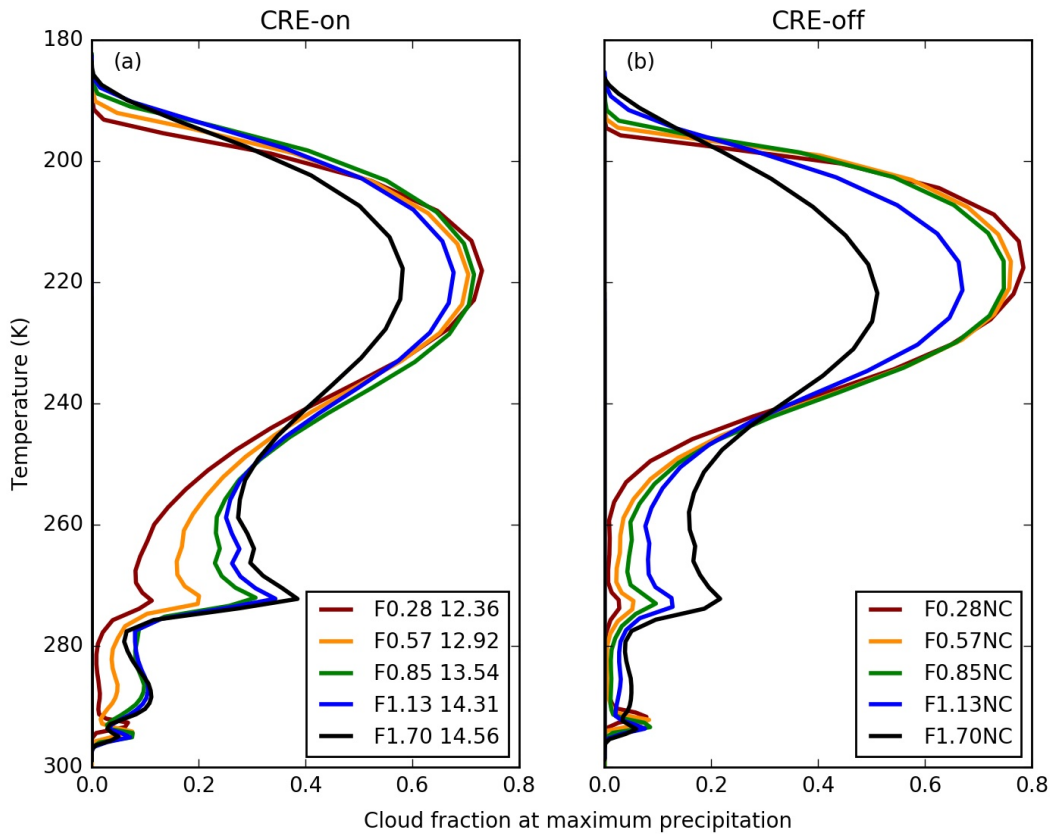
783 FIG. 5. Zonal-, time-mean mass meridional streamfunction ( $\text{kg s}^{-1}$ ) (lined contours) and vertical wind speed  
 784 ( $\text{m s}^{-1}$ ) (filled contours). Lined contours are in intervals of  $5 \times 10^{10}$ , with dashed contours representing negative  
 785 values. Dotted contour is zero value. (a) F1.70NC, (b) F1.13NC, (c) F0.85NC, (d) F0.57NC, (e) F0.28NC.  
 786 Maximum value of the mass meridional streamfunction printed in top right-hand corner of each subplot.



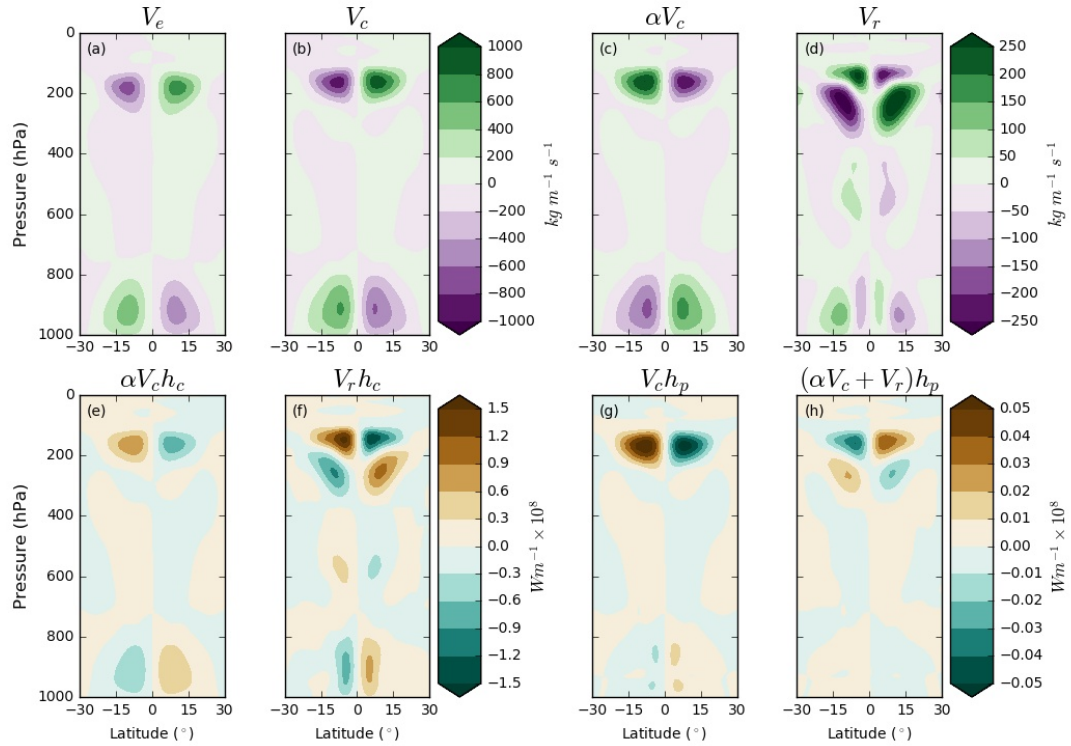
787 FIG. 6. Zonal, time-mean AEI components ( $\text{W m}^{-2}$ ). (b) F1.13NC (a),(c)-(e): Change in AEI components  
788 compared to F1.13NC for (a) F1.70NC; (c) F0.85NC, (d) F0.57NC, (e) F0.28NC and (f): Change in AEI compo-  
789 nents when removing cloud-radiation interactions at  $f_{dp}$  equals 1.13 (F1.13NC - F1.13). Note, (a) and (c)  
790 have axis limits  $-20$  and  $20 \text{ W m}^{-2}$  whilst (d)-(f) have limits  $-80$  and  $80 \text{ W m}^{-2}$ .



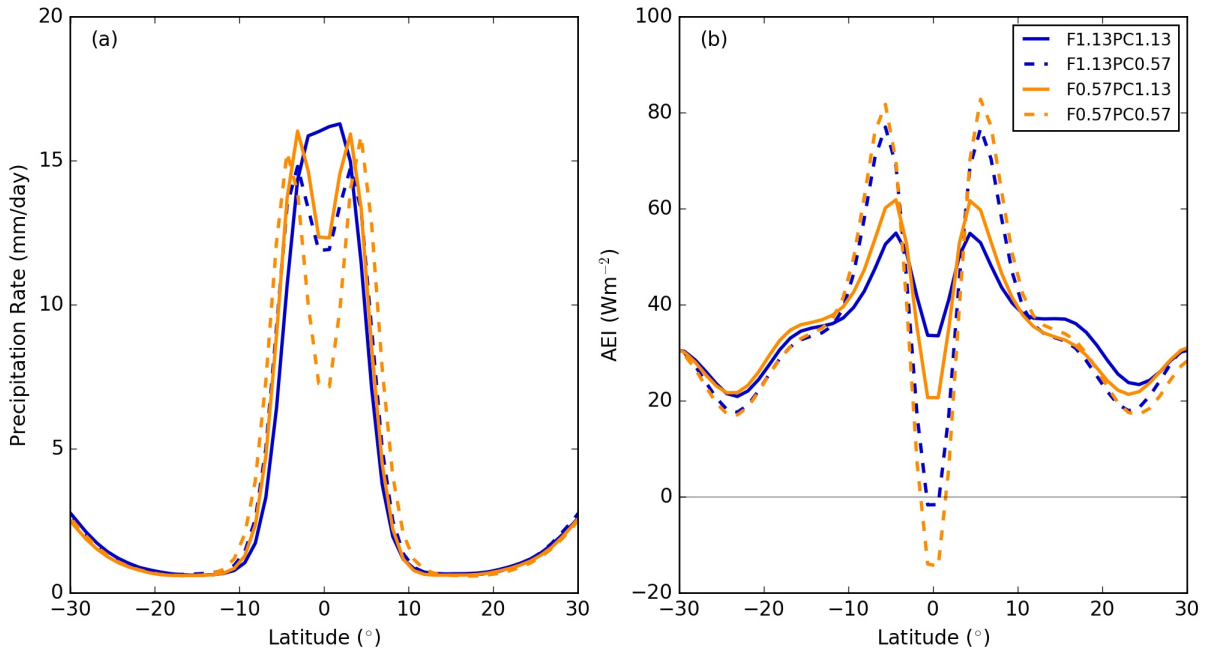
791 FIG. 7. Diagnostics for determining the sensitivity of the ITCZ to  $f_{dp}$  in CRE-on (green) and CRE-off (blue)  
 792 simulations. Top (a): Latitude of maximum precipitation ( $^{\circ}$ ), bottom (b): Precipitation rate at ITCZ (mm day<sup>-1</sup>).  
 793 Four regression lines are plotted in each subplot. Solid lines where  $0.28 \leq f_{dp} \leq 1.13$  and dashed lines where  
 794  $f_{dp} \leq 1.70$ . The slope of each regression line is printed in the legend. First value where  $0.28 \leq f_{dp} \leq 1.13$  and  
 795 second value where  $f_{dp} \leq 1.70$ .



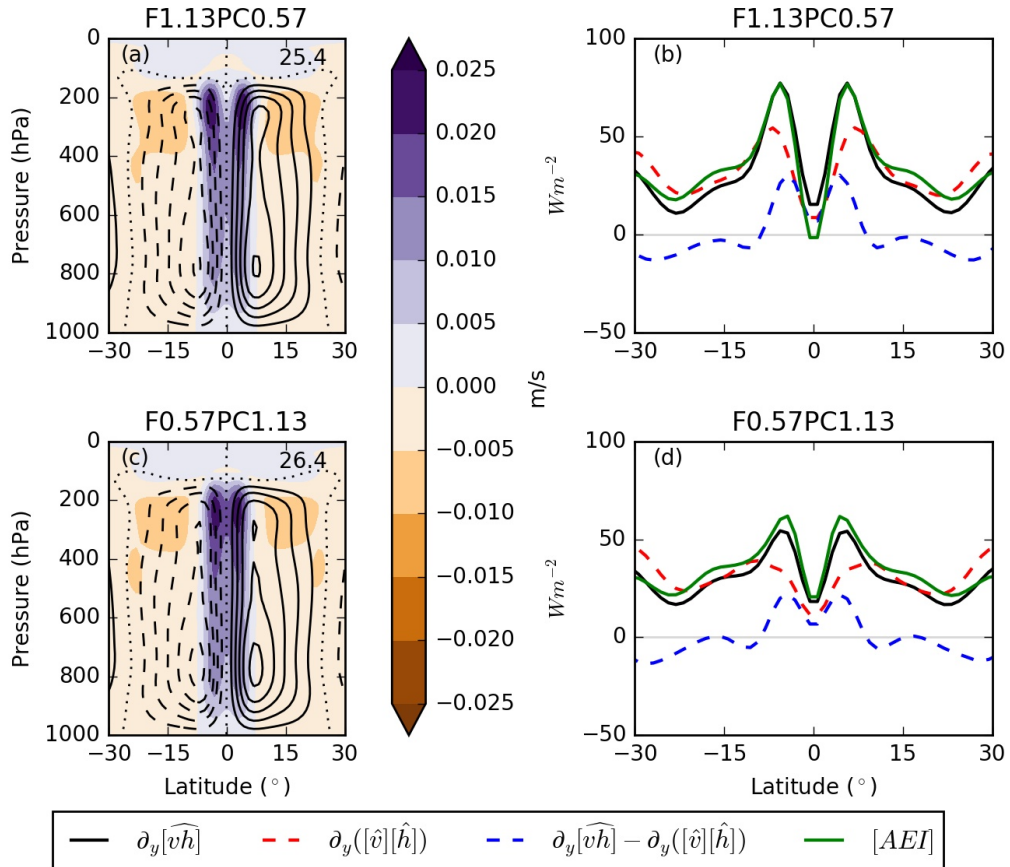
796 FIG. 8. Zonal-, time-mean cloud fraction against temperature (K) at latitude of maximum precipitation. Left  
 797 (a): CRE-on simulations, right (b): CRE-off simulations. Printed in legend, the tropical-domain average CRE  
 798 ( $\text{W m}^{-2}$ ) for CRE-on simulations.



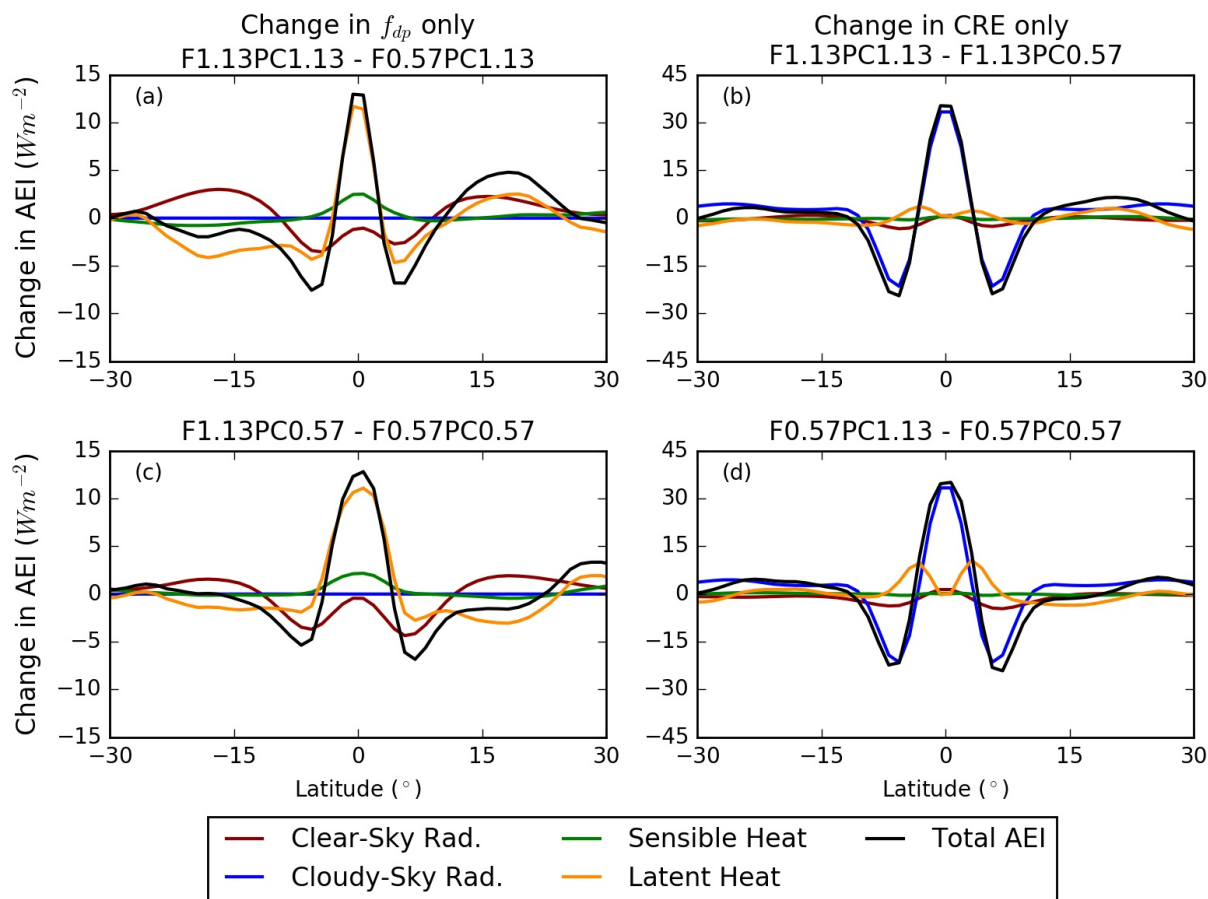
799 FIG. 9. Top row: (a) and (b): Meridional mass flux ( $\text{kg m}^{-1} \text{s}^{-1}$ ) in F1.13NC and F1.13 respectively, (c)  
800 and (d): Change in meridional mass flux due to change in circulation strength and change in meridional wind,  
801 respectively. Bottom row: Components of MSE flux change ( $\text{W m}^{-1}$ ), equation (10), due to (e), circulation  
802 intensity changes  $\alpha V_c h_c$ , (f), changes in circulation structure  $V_r h_c$ , (g), MSE profile changes  $V_c h_p$ , and, (h),  
803 MSE changes correlated with changes in circulation structure and strength  $(\alpha V_c + V_r) h_p$ . Analysis explained in  
804 Section 3c.



805 FIG. 10. Zonal-, time-mean (a) precipitation rates ( $mm day^{-1}$ ) and (b) AEI ( $W m^{-2}$ ) in simulations with a  
 806 prescribed CRE.



807 FIG. 11. Left: Zonal-, time-mean mass meridional streamfunction ( $\text{kg s}^{-1}$ ) (lined contours) and vertical wind  
 808 speed ( $\text{m s}^{-1}$ ) (filled contours) for (a) F1.13PC0.57 and (c) F0.57PC1.13. Lined contours are in intervals of  $5$   
 809  $\times 10^{10}$ , with dashed contours representing negative values. Dotted contour is zero value and maximum value of  
 810 the mass meridional streamfunction printed in top right-hand corner of each subplot. Right: Divergence of the  
 811 MSE flux ( $\text{W m}^{-2}$ ) and AEI for (b) F1.13PC0.57 and (d) F0.57PC1.13. Solid black line - Divergence of total  
 812 MSE flux  $\partial_y[\widehat{v\widehat{h}}]$ , red dotted line - MSE flux due to mean circulation  $\partial_y([\widehat{v}][\widehat{h}])$ , blue line -  $\partial_y[\widehat{v\widehat{h}}] - \partial_y([\widehat{v}][\widehat{h}])$ , green  
 813 line -  $[AEI]$ .



814 FIG. 12. Changes in zonal-, time-mean AEI contributions ( $\text{W m}^{-2}$ ) for prescribed CRE simulations. Com-  
 815 parison of simulations with same  $f_{dp}$  constant (a, c) have y-axis limits of  $-15$  to  $15 \text{ W m}^{-2}$ , whilst those with a  
 816 different prescribed CRE (b, d) have y-axis limits  $-45$  to  $45 \text{ W m}^{-2}$ .